Journal of South American Earth Sciences 106 (2021) 103045

Contents lists available at ScienceDirect

Journal of South American Earth Sciences

journal homepage: www.elsevier.com/locate/jsames

Igneous-metamorphic basement of Taquetrén Range, patagonia, Argentina: A key locality for the reconstruction of the paleozoic evolution of patagonia

Emiliano M. Renda [a,*], Pablo D. González [b], Haroldo Vizán [a], Sebastián Oriolo [a], Claudia Prezzi [a], Víctor Ruiz González [a], Bernhard Schulz [c], Joachim Krause [d], Miguel Basei [e]

[a] CONICET-Universidad de Buenos Aires. Instituto de Geociencias Básicas, Aplicadas y Ambientales de Buenos Aires(IGEBA), Intendente Güiraldes 2160, C1428EHA, Buenos Aires, Argentina
[b] Instituto de Investigación en Paleobiología y Geología, UNRN-CONICET, Av. Julio A. Roca 1242, R 8332 EXZ, General Roca, Río Negro, Argentina
[c] Institute of Mineralogy, Division of Economic Geology and Petrology, TU Bergakademie Freiberg, Freiberg/Saxony, Germany
[d] Helmholtz-Zentrum Dresden-Rossendorf, Helmholtz Institute Freiberg for Resource Technology, Freiberg, Germany
[e] Centro de Pesquisas Geocronológicas, Instituto de Geociências, USP, Rua do Lago 562, CEP 05508-080, São Paulo, SP, Brazil

ARTICLE INFO

Keywords:
Patagonia
Paleozoic
Igneous-metamorphic basement
U–Pb zircon
Th–U–Pb monazite

ABSTRACT

In this contribution, we present the stratigraphy of the igneous and metamorphic rocks of the Taquetrén Range, a sector located in the southernmost margin of the North Patagonian Massif (42°42′00″ S - 69°30′00″ W). Its igneous and metamorphic basement is composed of the newly defined "Lagunita Salada Igneous-Metamorphic Complex" (LSIMC), "Paso del Sapo Plutonic Complex" (PSPC) and "Sierra de Taquetrén Plutonic Complex" (STPC). The LSIMC comprises gneisses, schists, amphibolites and migmatites, which share a S_1–S_2 penetrative foliation with a mean orientation of 300°–330°/40°–60° NE. Based on mineral paragenesis, metamorphic conditions of these rocks are the result of Barrovian-type metamorphism in the upper amphibolite to granulite facies. EPMA Th–U–Pb ages of monazites display two isochron main populations at 379 ± 5 Ma and 323 ± 5 Ma, which suggest long-term high-temperature conditions for the region between Late Devonian and Carboniferous times. The Complex is intruded by concordant tonalites, granodiorites, porphyric granites and minor pegmatites and felsic dykes, which are grouped in the PSPC. Both the LSIMC and PSPC are intruded by unfoliated peraluminous granitoids grouped in the STPC. Based on field and microstructural data, the pervasive foliation identified in the PSPC was caused by processes ranging from magmatic flow to solid-state deformation, indicating a syntectonic emplacement. Zircon U–Pb analysis by LA-ICP-MS in the PSPC shows two distinguishable groups with concordia ages of 314.1 ± 2.2 Ma and 302.8 ± 2.2 Ma, interpreted as the crystallization and subsequent deformation age respectively, related to protracted high-strain conditions. The outcrops in this area represent an almost full tectonic cycle encompassing from medium-high grade metamorphic rocks and syn-tectonic intrusions to post-tectonic intrusions, therefore configuring a key locality for the analysis of North Patagonian Paleozoic evolution. Moreover, based on the compilation of U–Pb zircon ages, a ~20 My magmatic gap period (360-340 Ma) is recognized in the southwestern margin of the North Patagonian Massif coeval with amphibolite-granulite facies metamorphism in different sectors of the Central Patagonian Igneous-Metamorphic Belt, presenting thus important implications for the tectonic evolution of the area.

Author statement

Renda Emiliano M.: Conceptualization, Investigation, Data curation, Visualization, Writing. Pablo D. González: Conceptualization, Writing – review & editing. Haroldo Vizán: Conceptualization, Funding acquisition, Writing – review & editing Sebastián Oriolo: Methodology, Funding acquisition, Writing – review & editing. Claudia Prezzi: Funding acquisition Writing – review & editing. Victor Ruiz González: Writing – review & editing. Bernhard Schulz: Methodology, Writing – review & editing. Joachim Krause: Methodology. Miguel Basei: Methodology, Funding acquisition.

* Corresponding author. Intendente Güiraldes, 2160, C1428EHA Buenos Aires, Argentina.
E-mail address: renda.emi@gmail.com (E.M. Renda).

https://doi.org/10.1016/j.jsames.2020.103045
Received 28 June 2020; Received in revised form 13 November 2020; Accepted 17 November 2020
Available online 28 November 2020

1. Introduction

Convergent plate margins are the main tectonic setting where continental crustal growth occurs. The major contribution to crustal growth in these areas is given by the underplating of basaltic magmas derived from the mantle and the generation of granulite terranes in the upper plate by crustal thickening and related metamorphism (Fountain and Salisbury, 1981; Bohlen and Mezger, 1989; Yoshino and Okudaira, 2004). Therefore, assessing the tectonometamorphic evolution and timing of thickening processes that occurred in ancient orogenic belts is a crucial factor for understanding and reconstructing the crustal growth history in a certain area.

In southern South America, a series of Paleozoic orogenic belts, separating discrete crustal blocks, have been identified and assigned to different collisional and accretional events that contributed to the crustal growth and evolution of the South American plate. One of these distinct blocks is the North Patagonian Massif, which has been alternatively considered as part of the Gondwanan margin since Early Paleozoic (Pankhurst et al., 2006; Rapalini et al., 2013; Pankhurst et al., 2014; Vizán et al., 2017; Prezzi et al., 2018; González et al., 2018, among others) or since Late Paleozoic times (Ramos, 1984; Ramos, 2008; Pángaro and Ramos, 2012; among others). Besides the paleogeographic location of the North Patagonian Massif, its tectonic evolution during the Paleozoic is still unclear.

In the last decades an orogenic belt, proposed as a potential suture zone and formed by middle to late paleozoic plutonic and metamorphic rocks, was defined in the southwestern boundary of the North Patagonian Massif showing a regional NW-SE structural trend (Pankhurst et al., 2006; Ramos, 2008; Varela et al., 2015; Renda et al., 2019) which affects the late geological evolution of the region (Giacosa and Heredia, 2004; Figari, 2005; Bilmes et al., 2013; Echaurren et al., 2016; Zaffarana et al., 2017; Bucher et al., 2019; Foix et al., 2020; Renda et al., 2019; Suarez et al., 2019; Ruiz González et al., 2020; Giacosa et al., 2020). In this area, different basement lithologies are found; however, they have not been studied in detail and geochronological data is only limited to specific sectors, thereby limiting the understanding of the geological processes that occurred along this potential paleozoic plate margin. In this sense, the scarcity of robust constraints on the timing and characteristics of deformational and metamorphic processes in the North Patagonian Massif appears as a significant limitation for paleogeographic reconstructions and for the assessment of the tectonometamorphic history in this area.

Therefore, the aim of this paper is to present the stratigraphy of the igneous and metamorphic basement rocks that crop out in Paso del Sapo area (central area of the orogenic belt) and surroundings (Taquetrén range), so far mostly unexplored, which belongs to the southernmost margin of the North Patagonian Massif (42°42′00”S-69°30′00”W, Chubut province, Fig. 1). Moreover, a chronologic sequence of deformational structures and associated metamorphic conditions from selected key outcrops are also presented. Qualitative information about P-T conditions of regional metamorphism is assessed by using mineral assemblages and reaction microstructures, whereas new U–Pb zircon and monazite ages of igneous and metamorphic rocks respectively, were obtained in order to constrain the timing of magmatic crystallization and metamorphism-deformation. The obtained results are combined with already published data in order to infer a schematic tectonometamorphic and magmatic evolution of the igneous-metamorphic belt extending along the southernmost margin of the North Patagonian Massif.

2. Regional geological setting

The North Patagonian Massif is a ~100.000 km^2 geological region located in the northern part of Argentinean Patagonia (Fig. 1). In its northeastern sector, a Cambro-Ordovician igneous-metamorphic basement is overlain by Silurian orthoquartzites deposited in a passive margin setting (Ramos, 1975; Caminos, 1983; Giacosa, 1987; Busteros et al., 1998; Uriz et al., 2011; Greco et al., 2015; González et al., 2018). By contrast, the basement in the southwestern boundary of the North Patagonian Massif is formed by Middle to Upper Paleozoic igneous and metamorphic units (Varela et al., 2005, 2015; Pankhurst et al., 2006;

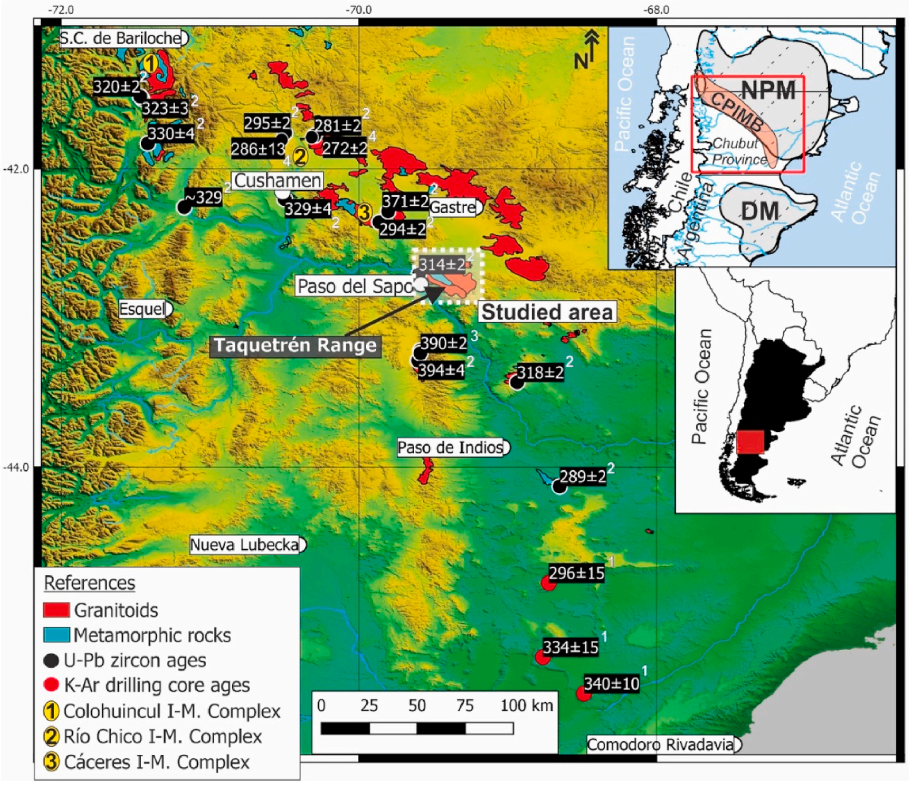

Fig. 1. Geological sketch map of the southwestern area of the North Patagonian Massif (NPM) showing the main paleozoic basement outcrops and the available U–Pb zircon crystallization ages of plutons (black dots). The studied area (Taquetren range) is indicated. Red dots represent K–Ar ages of basement rocks obtained from drilling cores. Ages from 1. K–Ar ages (Lesta, 1980; Linares and González, 1990). U–Pb ages from 2. Pankhurst et al. (2006), 3. Hervé et al. (2018), 4. Varela et al. (2005). NPM: North Patagonian Massif, DM: Deseado Massif, CPIMB: Central Patagonian Igneous-Metamorphic Belt. (For interpretation of the references to color in this figure legend, the reader is referred to the Web version of this article.)

Ramos, 2008), exposed along the Western Magmatic Arc (Ramos, 2008) or the paleozoic Central Patagonian Igneous-Metamorphic Belt (Renda et al., 2019, Fig. 1). This igneous-metamorphic belt is limited in its western part by the Early Carboniferous-Permian marine-continental Tepuel Basin (Limarino and Spalletti, 2006) and its sedimentary supply was associated with a magmatic arc located either on the western area of North Patagonian Massif or in the Chilean accretionary prism (Ciccioli et al., 2020).

The studied area is located in the southwestern boundary of North Patagonian Massif, in the Patagonides belt, which comprises a NW-SE oriented mountain range with a mean altitude of 1200 m, located in the central area of extra-Andean Patagonia (Ramos, 1999). This mountain range is primarily developed by fault-controlled basement blocks overlaid by inverted Mesozoic - Cenozoic depocenters, covered by tertiary basalt plateaus (Folguera and Ramos, 2011; Bilmes et al., 2013). Different names have been given to the Andean and extra-Andean basement units. In the extra-Andean region, the metamorphic basement and associated plutonic rocks have been classically grouped under the medium-high metamorphic grade Cushamen Formation (Volkheimer, 1964) and the plutonic Mamil Choique Formation (Ravazzoli and Sesana, 1977), respectively. In the Andean region, near San Carlos de Bariloche, metamorphic rocks have been assigned to the Colohuincul Complex (reference 1 in Fig. 1) while associated plutonic rocks are grouped in the Huechulafquen Formation (Turner, 1965). Nevertheless, different igneous-metamorphic complexes have been defined in specific sectors of the Central Patagonian Igneous-Metamorphic Belt, namely, Río Chico (Dalla Salda et al., 1994; reference 2 in Fig. 1) and Cáceres Igneous-Metamorphic Complexes (Giacosa et al., 2014; reference 3 in Fig. 1). This approach is followed in this paper for the definition of the new basement units located in the Taquetrén range, Chubut Province.

The Río Chico Complex is located near the homonymous locality (reference 2 in Fig. 1) and comprises medium-to high-grade schists, gneisses, migmatites and minor mica-rich quartzites interlayered with orthogneisses and minor intrusions (Dalla Salda et al., 1994; Cerredo and López de Luchi, 1998; Giacosa et al., 2004). The main metamorphic foliation strikes ~ NW-SE and associated foliated granitoids include a 329 ± 4 Ma hornblende-biotite granodiorite (Pankhurst et al., 2006), a foliated tonalite with 286 ± 13 Ma and 295 ± 2 Ma ages (Pankhurst et al., 2006; Varela et al., 2005) and a foliated leucogranite of 302 ± 39 Ma (Varela et al., 2005). On the other hand, the Cáceres Igneous-Metamorphic Complex includes high-grade schists, paragneisses, minor amphibolites and orthogneisses (reference 3 in Fig. 1, Giacosa et al., 2014). Metamorphic rocks exhibit a main metamorphic foliation striking NE-SW and are associated with syntectonic mylonitic granites yielding a 371 ± 2 Ma crystallization age, being intruded by post-tectonic granites with a 294 ± 2 Ma age (Pankhurst et al., 2006; Giacosa et al., 2014).

Igneous-metamorphic basement rocks of Paso del Sapo study area are pre-Jurassic and belong to the southernmost outcrops of the North Patagonian Massif (Fig. 2). The syn-rift (Hettangian-Kimmeridgian) and post-rift (Barremian-Danian) volcano-sedimentary mega-sequences of the Cañadón Asfalto basin (Fígari et al., 2015 and references therein) unconformably lie over the eroded basement rocks. Tertiary basalts and volcaniclastic deposits overlie both the basement rocks and the Jurassic-Cretaceous volcano-sedimentary cover. Regionally, the earliest mentions of the igneous and metamorphic basement rocks were made by Feruglio (1949, and references therein for a summary), whereas Nakayama (1973) mentioned the gneisses and granitoids of the Taquetrén range, as part of the Sierra de Taquetrén Formation, with no precise definition of these units. The structural and magnetic fabric studies of Paso del Sapo granodiorite (314 ± 2 Ma; Pankhurst et al., 2006) revealed a penetrative NW-SE-trending tectonic foliation dipping mostly to the NE (Renda et al., 2017, 2019).

3. Geology of Taquetrén Range basement

The main stratigraphic features of the area are derived from our field mapping since very few studies were previously carried out in the region (Section 2). Based on field relations and new geochronological constraints presented below (Section 3, 4, and 5), the crystalline basement of the Taquetrén Range was thus divided into three main complexes. Sequentially, from older to younger units, they correspond to the Lagunita Salada Igneous-Metamorphic Complex (LSIMC), Paso del Sapo Plutonic Complex (PSPC), and Sierra de Taquetrén Plutonic complex

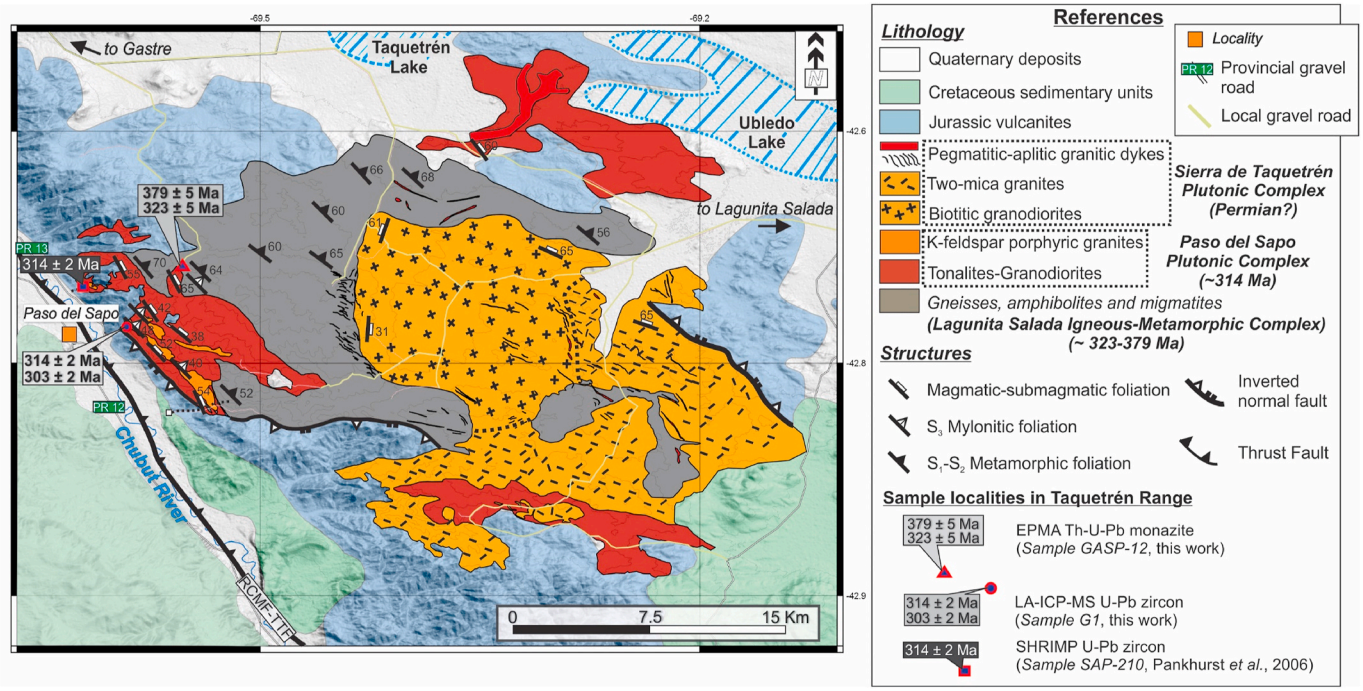

Fig. 2. Geological map of the studied area, the Taquetrén range located in central Patagonia, Argentina. Ages obtained in this work are shown along with previous ages obtained in the area. RCMF-TTF: Río Chubut Medio Fault – Taquetrén Thrust Front.

(STPC, Fig. 2). In this section, stratigraphic features are described for each complex, from data collected in key selected outcrops. Mineral abbreviations used in this work are based on Whitney and Evans (2010).

3.1. Lagunita Salada Igneous-metamorphic complex (LSIMC)

It comprises paragneisses, schists, amphibolites, minor orthogneisses, and migmatites. Its main outcrop area is located in the northern sector of the Taquetrén range (Fig. 2). The complex is intruded by tonalites and granodiorites of the Paso del Sapo Plutonic Complex (PSPC), parallel to the main fabric of the metamorphic rocks. The concordant intrusive contact is NW/SE-trending and dipping 35° to the NE (Fig. 3a). Within the contact aureola, a fine-grained granoblastic microstructure overprinted the previous gneissic foliation in paragneisses.

The LSIMC is, in turn, intruded with a discordant contact relationship by the granitoid plutons of the Sierra de Taquetrén Plutonic Complex (Fig. 2, STPC). Close to the contact zone between LSIMC and STPC, pegmatitic and aplitic granitic dykes of the STPC intrude with concordant and discordant relationships the pre-existing foliation of the LSIMC (Fig. 2).

The LSIMC is essentially composed of alternating medium to coarse-grained sillimanite-garnet paragneisses and fine-grained garnet mica schists (Fig. 3b). Paragneisses are grey-colored and show a well-developed S_1–S_2 gneissic penetrative foliation with a mean value of S_{1-2}: N 315°/64° NE (Fig. 3b). Stretched biotite and sillimanite define a NE-plunging, stretching lineation. Commonly, garnet is present as subhedral and anhedral syntectonic porphyroblasts. In some sectors, near the contact with the PSPC, the S_1–S_2 foliation presents an approximate curvilinear fabric, and asymmetric garnets show a sinistral (normal) sense of shear (Fig. 3c and 3.d).

The schists show a well-developed S_1–S_2 schistosity, parallel to the gneissic foliation, and they commonly exhibit grayish to greenish color due to retrograde chlorite formation at the expense of biotite (Fig. 3b). Few bodies of fine-grained amphibolites, up to 3 m-thick and with poorly developed S_1–S_2 foliations, are interlayered with paragneisses and schists. Migmatites are stromatic metatexites found in close association with paragneisses. The leucosomes are centimeter-thick tabular layers alternating with well-foliated biotite-rich mesosomes and lying parallel to the regional foliation S_1–S_2 (Fig. 3e). They are composed of medium to coarse-grained granoblastic quartz + plagioclase, with boudinaged structure (Fig. 3e).

3.1.1. Structures of the Lagunita Salada Igneous-Metamorphic complex

The complex is affected by three tectono-metamorphic events with regional distribution in the Taquetrén range. During D_1-D_2 coaxial events, pelite-psammite bedding S_0 was folded around SW-verging, overturned tight to isoclinal F_1–F_2 folds (Fig. 4a and b). The S_1

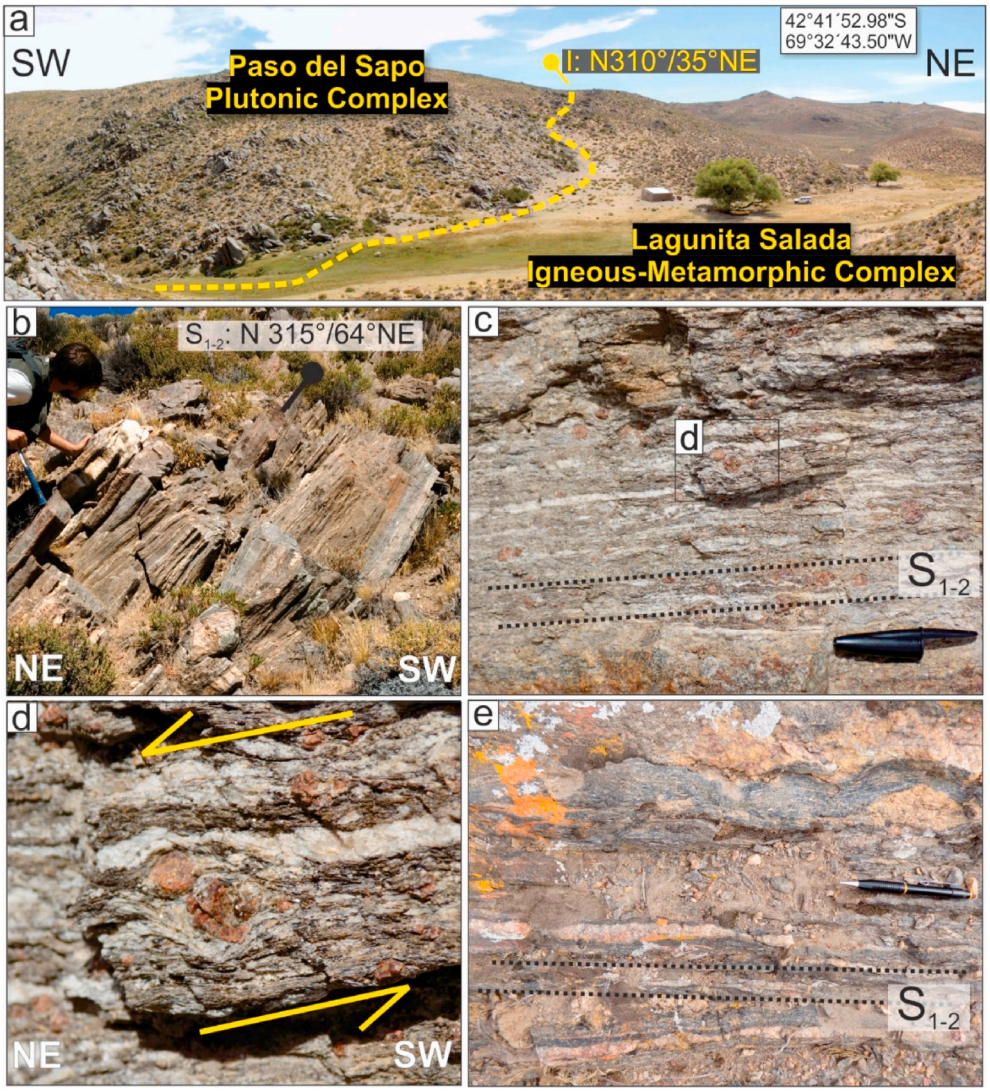

Fig. 3. a) Intrusive relationship between Paso del Sapo Plutonic Complex and Lagunita Salada Igneous-Metamorphic Complex. The contact plane strikes N 310° and dips 35° to the NE. b) S_1–S_2 metamorphic foliation developed in paragneisses of the Lagunita Salada Igneous-Metamorphic Complex. Thin layers of schists are intercalated between the paragneisses. c) Detailed outcrop view of the S_1–S_2 gneissic foliation. Subhedral garnets porphyroblasts are bordered by biotite and sillimanite. d) Detail of garnet porphyroblast within gneissic layering in paragneisses of the Lagunita Salada Igneous-Metamorphic Complex. The asymmetry of garnets tails indicates a sinistral sense of shearing. e) Metatexitic paragneisses. Boudinage structures are developed in the leucosomes.

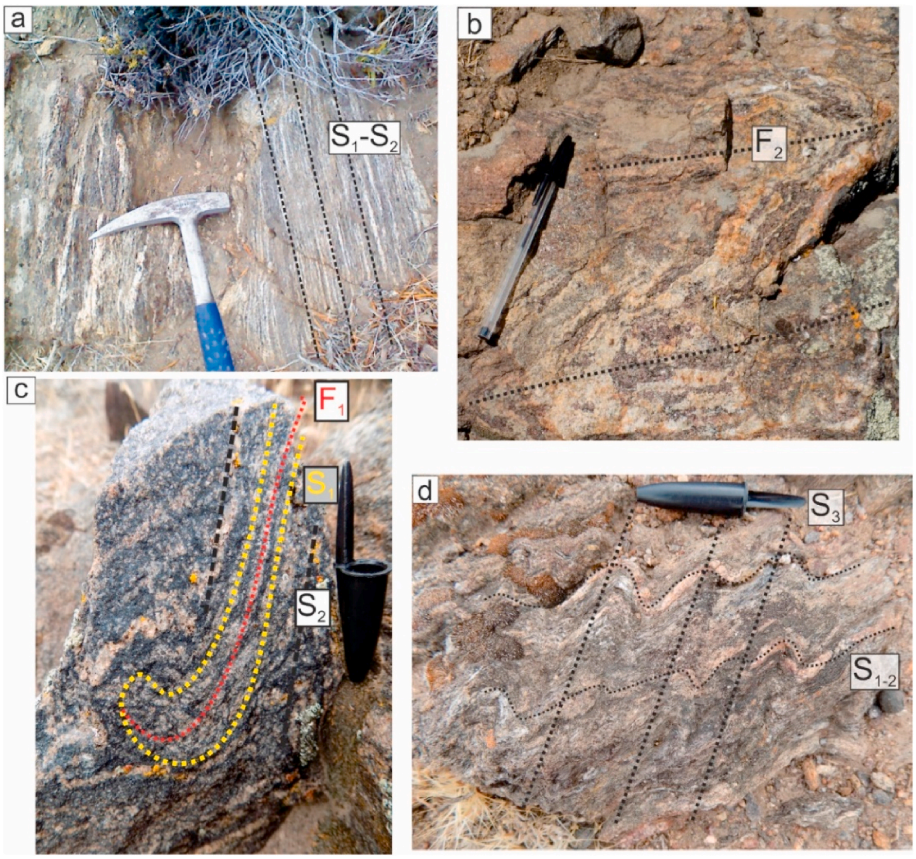

Fig. 4. Structural elements of the LSIMC and PSPC. a) S_1–S_2 gneissic foliation developed in paragneisses. b) Tight F_2 folds developed in paragneisses of LSIMC. c) Type-3 interference pattern formed by the refolding of F_1 isoclinal folds. d) Penetrative crenulation S_3 affecting S_1–S_2 foliation. Asymmetric crenulation folds are shown.

gneissic foliation defined by alternating dark and light-colored bands is relict and preserved in isoclinal F_1 folds (Fig. 4c). F_1 folds are refolded by F_2 folds (Type-3 interference pattern folds of Ramsay, 1967, Fig. 4c). F_2 folds are associated with a penetrative NW-SE trending axial plane foliation $S_{1\text{-}2}$: N315°-350°/30°-72°NE. Linear structures in the LSIMC include fold axis, mineral stretching lineations, and boudin axis. F_2 fold axes exhibit a mean orientation of F_2: N130°/40°. Mineral stretching lineations ($L_{1\text{-}2}$) are defined by elongated biotites and sillimanites with major axis oriented $L_{1\text{-}2}$: N019°-004°/61°–41°. Boudinage of leucocratic layers can be seen along the limbs of tight to isoclinal F_2 folds (Fig. 4b and c) or in individual leucosomes within the paragneisses.

D_3 structures are represented by a crenulation cleavage S_3 assocated with centimetric, tight to close F_3 asymmetric folds affecting S_1–S_2 (Fig. 4d). F_3 fold axis has a mean orientation of E_3: N 265°/43°. A retrograde mineral association developed in the F_3 hinge axis is defined by chlorite-sericite-muscovite alignment.

3.1.2. *Microstructure and metamorphism*

At a microscopic scale, two leading mineral associations M_1-M_2 were identified: (1) quartz-plagioclase-biotite-garnet-sillimanite, and (2) quartz-plagioclase-biotite-garnet-kyanite-sillimanite-K/feldspar-rutile. M_1 metamorphic association cannot be defined in the samples collected as it is obliterated by M_2. The S_1–S_2 foliation planes are marked by the preferred orientation of fibrolitic sillimanite and biotite flakes, alternating with quartz-feldspathic granoblastic micro-bands.

Reddish-brown biotite is typical to those from higher-metamorphic grades, whereas garnets occur as euhedral to subhedral porphyroblasts, up to 1 mm in diameter, with inclusion trails of quartz, apatite, and biotite, which are parallel to S_1–S_2 foliation planes of the matrix (Fig. 5a). Granoblastic bands are composed of fine-to medium-grained quartz + plagioclase with interlobate to polygonal contacts (Fig. 5b). Some quartz grains exhibit undulose extinction and tapered twins in plagioclase, associated probably with D3 event under low-grade metamorphic conditions. Fibrolitic sillimanite needles are parallel to biotite in lepidoblastic bands or anastomosed around coarse-grained granoblastic bands (Fig. 5c and d).

In the southern sector of the Taquetrén range, quartz-plagioclase-biotite-garnet-kyanite-sillimanite-K/feldspar-rutile mineral association M_1-M_2 in paragneisses marks the S_1–S_2 foliation planes, closely related with metatexitic migmatites. In kyanite-bearing paragneisses, relict S_1 garnet porphyroblasts located within S_1–S_2 bands are rimmed by fibrous sillimanite (Fig. 5e). Fine-grained, sub-idiomorphic kyanite is replaced by coronas of fibrous sillimanite (Fig. 5f). Prismatic sillimanite is intergrown with K-feldspar and in close relationship with biotite, within parallel oriented S_1–S_2 lepidoblastic bands (Fig. 5g).

Amphibolites are fine to medium-grained, with a well-developed S_1–S_2 metamorphic foliation defined by alternating bands of nematoblastic hornblende and granoblastic plagioclase + clino-pyroxene + orthopyroxene. Euhedral sphene forms coronas around opaque minerals (Fig. 5h), and apatite + zircons are scarce. The M_1-M_2 mineral assemblage is then defined as plagioclase-amphibole-clinopyroxene-orthopyroxene-sphene-opaque. Post-M_1/M_2 retrogression led to the development of chlorite around pyroxenes.

3.2. *Paso del Sapo Plutonic Complex (PSPC)*

The plutonic complex is mainly composed of biotite + amphibole-bearing tonalites, biotite ± amphibole-bearing granodiorites and porphyritic granites. Its most prominent outcrop is located in the western sector of the Taquetrén range, limited by the Río Chubut Medio

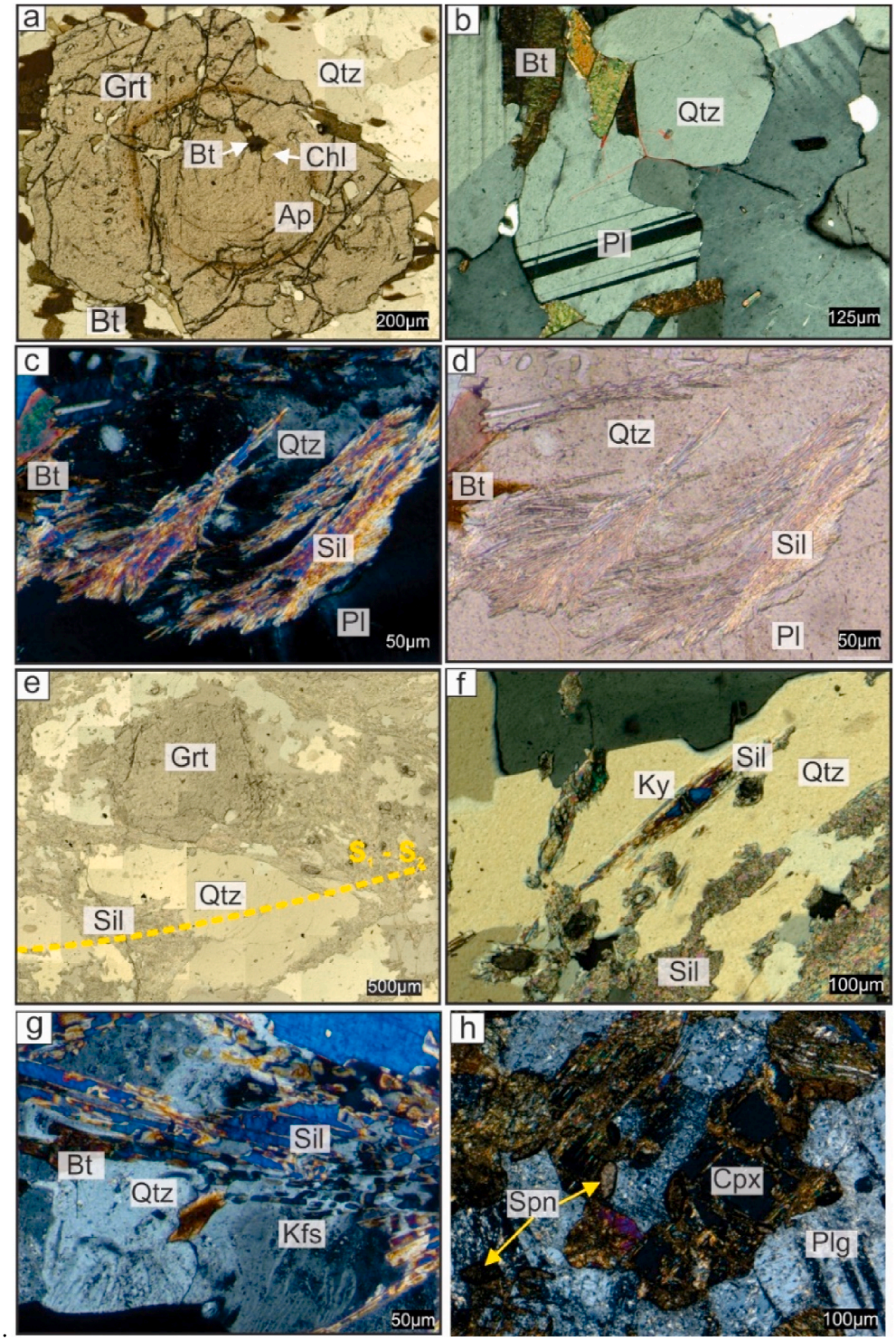

Fig. 5. Microscopic details of paragneisses of the Lagunita Salada Igneous-Metamorphic Complex. a) Subhedral garnet porphyroblast with visible zonation and inclusions of biotite, apatite and quartz. b) Quartz and plagioclase showing granoblastic microstructures and polygonal contacts. c and d) Fibrous sillimanite along with quartz and biotite. e) Garnet porphyroblast and fine-grained kyanite partially replaced by fibrous sillimanite. f) Individual kyanite replaced by fibrous sillimanite. g) Prismatic sillimanite, biotite and K-feldspar intergrowth. h) Clinopyroxene and sphene within plagioclase rich bands in amphibolites.

Fault-Taquetrén Thrust Front (RCMF-TTF in Fig. 2, Coira et al., 1975; Renda et al., 2019), and in the northeastern sector, by the Taquetrén and Ubledo lakes (Fig. 2). The PSPC presents an ovoid-shaped geometry, elongated in a NW-SE direction, parallel to the regional structural trend. Approximately 5 km to the northeast of the RCMF-TTF the complex intrudes with sharp and structurally concordant contacts the LSIMC. Although no field relations were found with the PSPC, the inclusions and xenoliths of these rocks into the Sierra de Taquetrén Plutonic Complex indicates that STPC intruded both already deformed complexes (see Section 3.3).

In mesoscale of the tonalites and granodiorites, shape-preferred biotite-amphibole-plagioclase orientation and recrystallized quartz aggregates parallel to them, define a penetrative magmatic to submagmatic foliation with a mean value of S_m: N 300°–330°/50° NE. Meter-sized granitic sheets intrude the tonalites and granodiorites with sharp to transitional contacts, and are parallel to the magmatic-submagmatic foliation planes (Fig. 6a). Centimeter-to meter-sized elongated and foliation-parallel metamorphic xenoliths of paragneisses from the LSIMC are common within the granodiorites (Fig. 6b). Discrete, meter-sized shear zones are well-defined within the plutonic complex

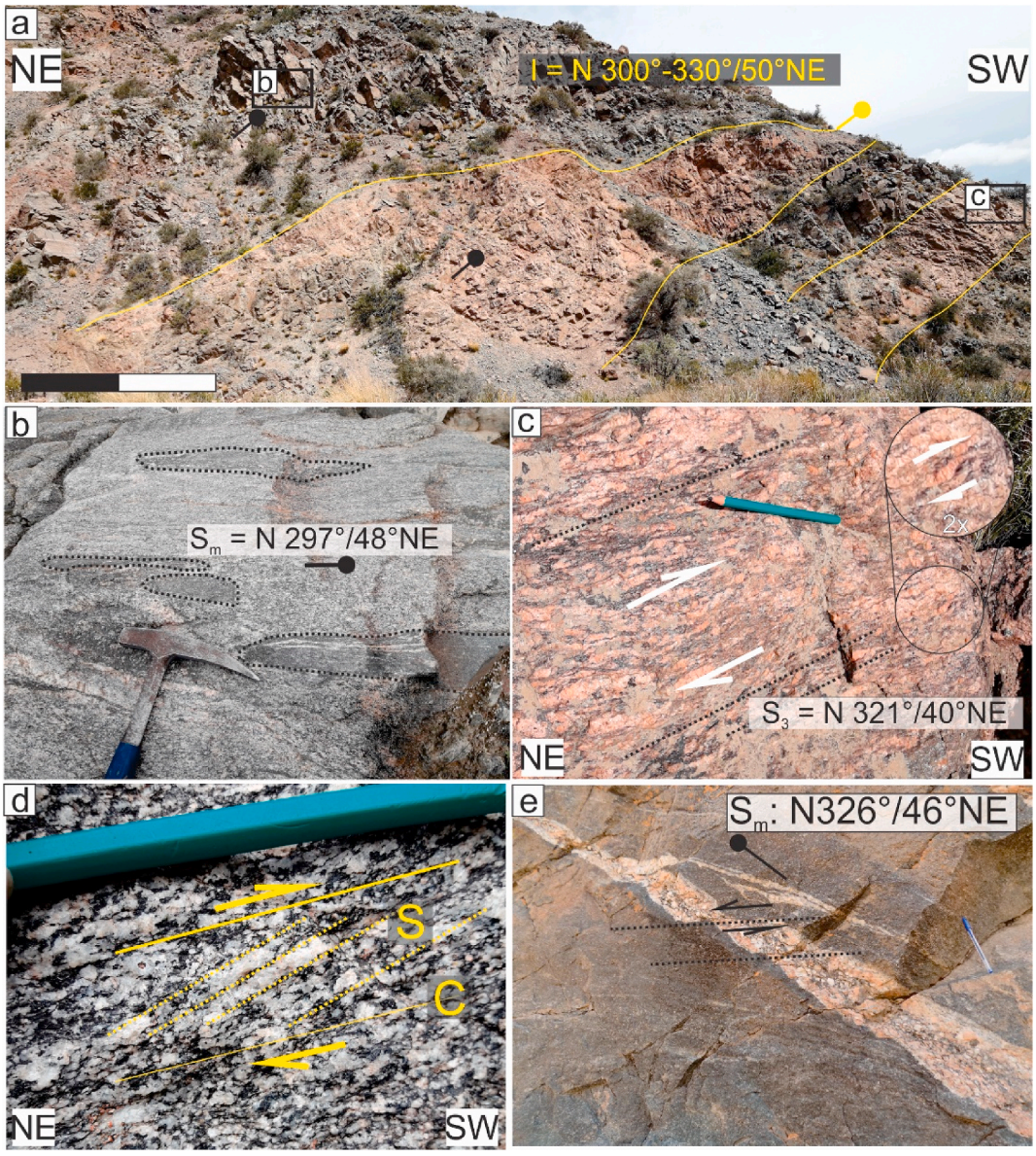

Fig. 6. Outcrops of the Paso del Sapo Plutonic Complex (PSPC). a) Alternation of tonalites and tabular-shaped intrusions of mylonitic K-feldspar megacrystal granites. I: igneous contacts between granodiorite and porphyric granite facies within the plutonic complex. S_m: Magmatic/submagmatic foliation. S_3: mylonitic foliation b) Solid-state foliation of the tonalite/granodiorite of PSPC with visible parallel-elongated metamorphic xenoliths. c) Mylonitic fabric developed in the K-feldspar megacrystal granites. The photograph points to the southeast and asymmetric K-feldspar crystals indicate a top-to-the-southwest tectonic transport direction. d) S–C structures developed in a granodiorite of the PSCP, indicating a dextral shear sense within a mylonitic shear zone. e) Synmagmatic faulting displacing tabular granitic intrusions.

and are visible at meso-scale. Within the shear zones, the NW-SE magmatic foliation is overprinted by an S_3 mylonitic foliation. Kinematic indicators, such as asymmetric σ-type K-feldspar porphyroclasts and S–C shear bands indicate a top-to-the-southwest tectonic transport direction (Fig. 6c and d). Synmagmatic deformation is represented by intramagmatic faults and shear zones which locally displace tabular granitic intrusions (Fig. 6e).

3.2.1. *Microstructures*

Tonalites are typically medium-grained, equigranular, with preferably oriented subhedral plagioclase, quartz aggregates, biotites, and hornblende. Zircon, apatite, titanite, and magnetite are present as accessory minerals. The granitoids developed a magmatic foliation (S_m) evidenced in the preferred alignment of subhedral hornblende and plagioclase crystals (Fig. 7a and b). Close to the mylonitic shear zones, a tectonic banding due to the transposition of previous planar structures resembles gneissose banding. In the mylonites, quartz occurs as medium- to fine-grained polycrystalline aggregates with irregular grain boundaries generated by grain boundary migration recrystallization (Fig. 7c). Also chessboard extinction patterns is common within the quartz aggregates, suggesting high-temperature solid-state deformation conditions. The polycrystalline aggregates are elongated and define a mylonitic foliation along with biotite flakes. Plagioclase (An_{30}-An_{70}) is present as medium-grained, subhedral crystals, commonly fractured, with irregular borders. Mylonitic granites show microcline porphyroclasts with wormy myrmekite lobes along the margins parallel to S_3 mylonitic foliation (Fig. 7d), suggesting a strain-controlled occurrence (Simpson and Wintsch, 1989), possibly related with medium/high-temperature submagmatic to solid-state deformation (Paterson et al., 1989; Simpson and Wintsch, 1989; Cisneros-Lazaro et al., 2019).

Asymmetric K-feldspar porphyroclasts show undulose extinction and

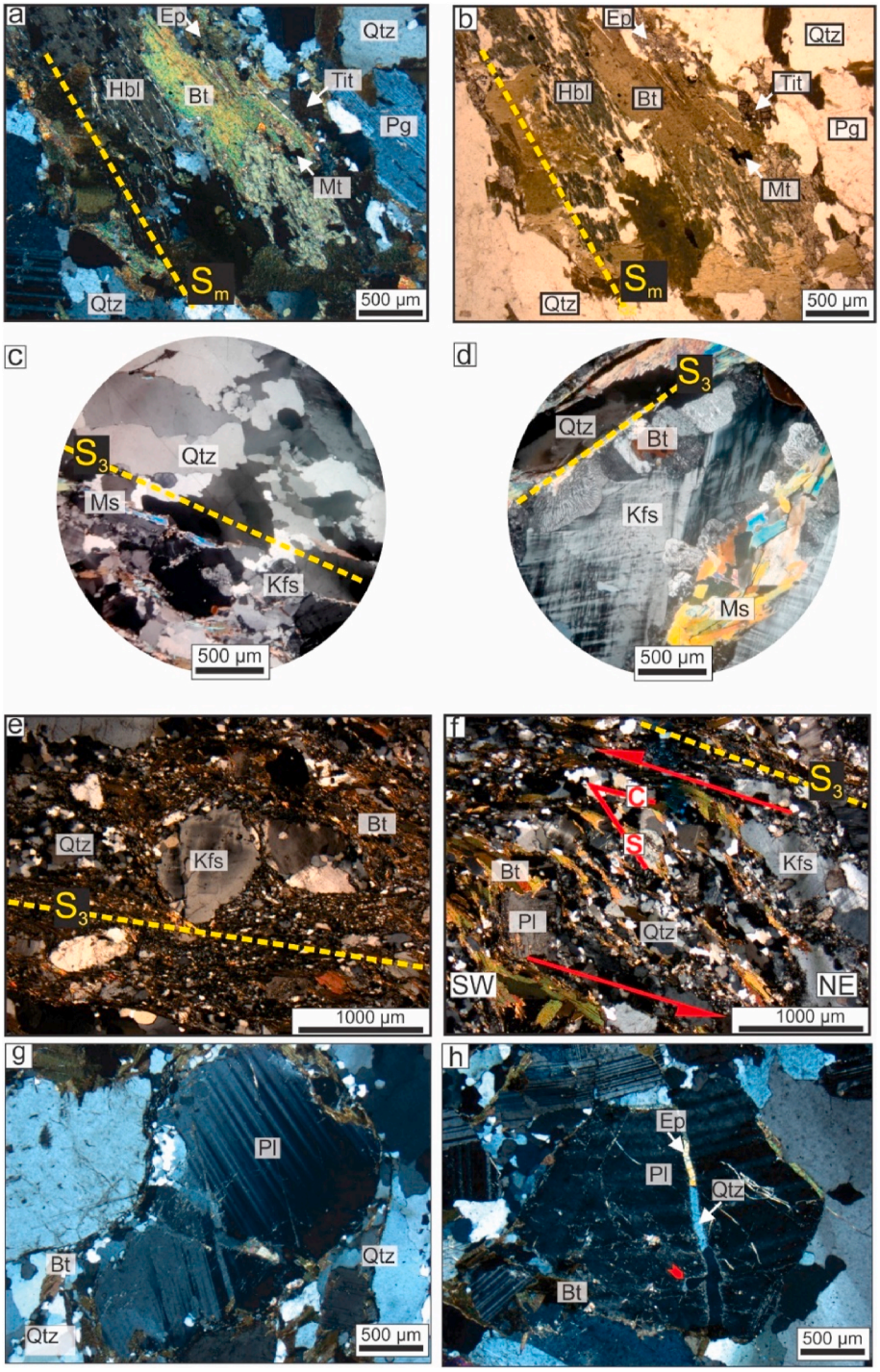

Fig. 7. Photomicrographs of the PSPC. a - b) S_m magmatic foliation defined by the alignment of hipidiomorphic hornblende and plagioclase, along with biotite, titanite, epidote and magnetite. Plane polarized light and under cross polarized light respectively. c) Pollycristaline aggregates of recrystallized quartz showing grain boundary migration and chessboard extinction patterns d) Hipidiomorphic microcline with myrmekites developed along grain margins parallel to S_3 mylonitic foliation. e) Allotriomorphic microcline with recrystallization to aggregates of quartz in "tail" region. The matrix consists of fine-grained recrystallized quartz, k-feldspar and biotite. f) S–C shear bands in the mylonitic porphyric granite of PSPC. g) Allotriomorphic plagioclase with fractures and wedge-shaped deformation twins. h) Submagmatic microfractures developed in an allotriomorphic plagioclase sealed by magmatic epidote and quartz. Red arrow shows a reabsorbed embayment within the fracture. (For interpretation of the references to color in this figure legend, the reader is referred to the Web version of this article.)

fine-grained recrystallized subgrains along boundaries. They are surrounded by a fine-grained matrix composed of biotite, quartz, and muscovite, and its major axis is parallel-oriented to S_3 mylonitic foliation (Fig. 7e). S–C shear bands related to S_3 mylonitic foliation are defined by mica-fish orientation of biotites and asymmetric recrystallized quartz aggregates, both indicating a top-to-the-southwest tectonic transport direction (Fig. 7f). Submagmatic microfractures (Bouchez et al., 1992), sealed by magmatic quartz and epidote, are present within plagioclase grains suggesting the presence of melt during late-stage brittle deformation (Fig. 7g and h).

3.3. Sierra de Taquetrén Plutonic Complex (STPC)

The STPC consists of three main facies of biotitic granodiorite, two-mica granites and pegmatites, and granitic dykes. The granitic facies was previously referred to as the Sierra de Taquetrén Formation by Nakayama (1973). Outcrops are typically rounded landforms of undeformed and non-foliated, light brown to grey, medium-grained granodiorites and granites, intruding the LSIMC with sharp and discordant contacts (Fig. 8a). Close to contacts with the LSIMC, centimeter to meter-sized pegmatite veins and granitic dykes are margin-parallel oriented or intrude concordantly the metamorphic foliation of the LSIMC (Fig. 8b). Roof pendants and stoped blocks of both the

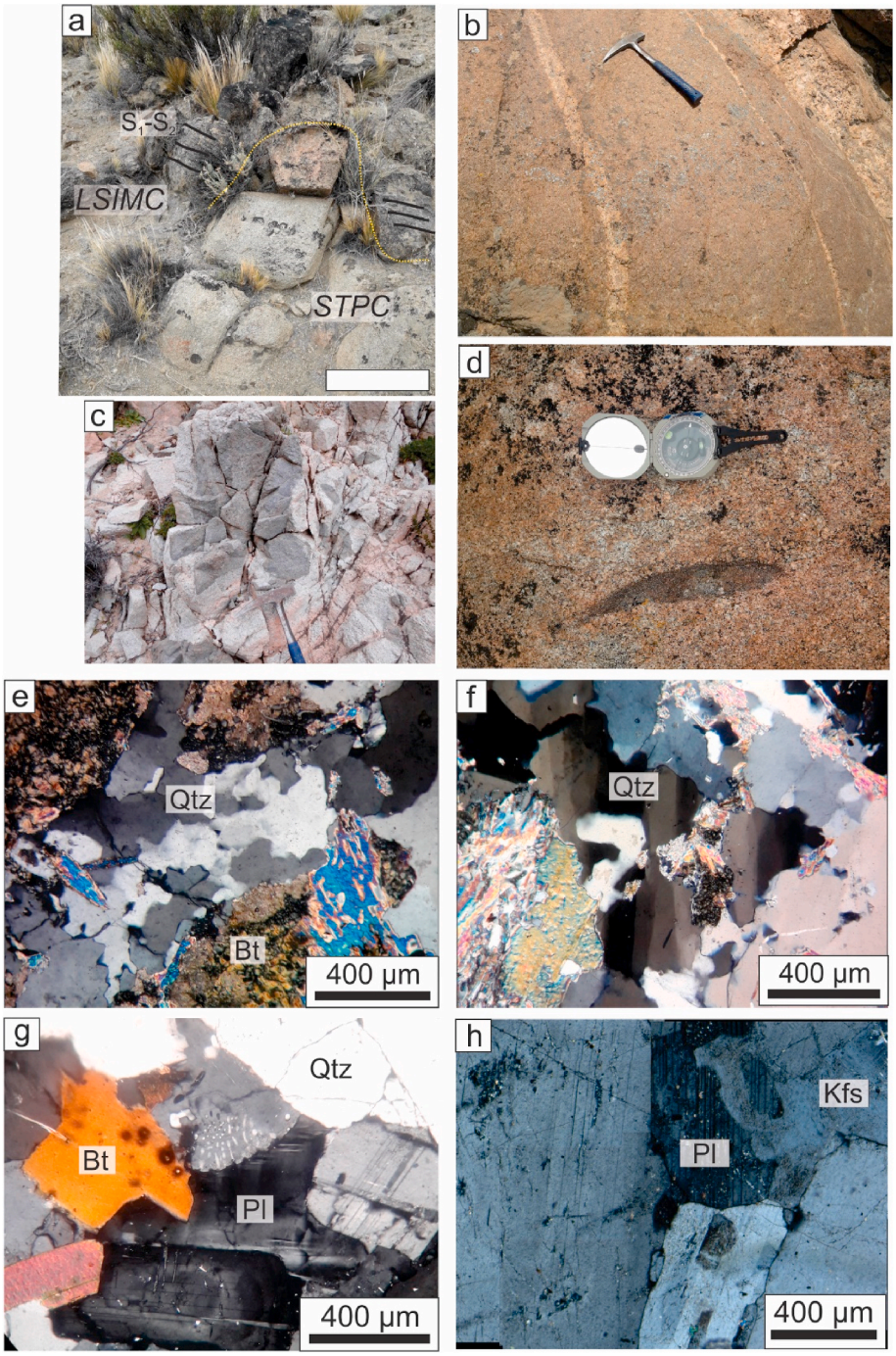

Fig. 8. Field and petrographic characteristics of the STPC. a) Sharp and discordant contact between STPC and LSIMC. The white scale is 30 cm long. b) Pegmatitic dykes and veins parallel disposed to the margins of the plutonic complex. c) Outcrop near the northern margin of the plutonic complex where an elongated mafic microgranular enclave is disposed with its major axis parallel to a roughly-defined magmatic foliation defined by the shape preferred orientation of biotites, k-feldspar and plagioclase. d) Stoped block of the PSPC within the STPC showing rectangular borders. e – h) Microstructures and petrography of the STPC. e) Solid state fabric showing lobate contacts developed in parallel-oriented quartz aggregates. f) Undulose extinction in quartz, show sharp transitions defining parallel elongated subgrains. g) Textural aspect of medium grained, equigranular, hypidiomorphic biotitic granodiorite facies. h) Plagioclase and K-feldspar intergrowth in the two-mica granite facies of the STPC.

metamorphic rocks and the granodiorites of PSPC lie along the margins of the body (Fig. 8c).

The STPC presents an irregular shape in the horizontal map section (Fig. 2) and lacks macroscopic internal structures, except near the borders where a blurred, contact-parallel magmatic foliation is developed, marked by elongated mafic microgranular enclaves with its major axis parallel-oriented to the incipient magmatic foliation (Fig. 8d). Solid-state deformation fabrics are present in the marginal zones of the plutonic complex, evidenced by microstructures showing lobate grain boundaries within quartz aggregates and recovery processes evidenced in the formation of quartz subgrain domains (Fig. 8e and f). These marginal zones are commonly altered, showing partial or total replacement of biotite by chlorite and secondary muscovite.

The granodiorite facies is formed by light brown, medium-grained (1–5 mm in diameter), equigranular biotitic granodiorites displaying an isotropic fabric (Fig. 8g). It is composed of quartz, plagioclase, K-feldspar, and biotite with minor epidote, allanite, apatite, opaques, and zircon. Quartz is present as anhedral, medium-grained crystals commonly fractured (Fig. 8g). Plagioclase is euhedral to subhedral, medium to coarse-grained, with well-developed twins and exhibiting zonation (Fig. 8g). Biotite is abundant, medium-grained, euhedral to subhedral crystals, with dark-brown/light-brown strong pleochroism, and numerous inclusions of zircons with pleochroic halos (Fig. 8g). K-feldspar is rare andoccurs as anhedral to subhedral crystals partially altered to sericite.

The granodioritic facies is mainly located in the western and southern sector of the plutonic complex (Fig. 2), and presents transitional contacts with the two-mica granite facies. The last consists of white to

grey-colored, medium-to-coarse-grained, hetero-granular hypidiomorphic granites, showing an isotropic fabric (Fig. 8h). It is mainly composed of quartz, K-feldspar, plagioclase, muscovite, and biotite. Plagioclase is present as a medium to coarse-grained, subhedral to euhedral crystals, with partial replacement of sericite and intergrowth textures with anhedral to subhedral K-feldspar (Fig. 8h). Epidote, apatite, zircon, and opaques are present as accessory minerals.

4. U–Pb geochronology

4.1. Samples and analytical techniques

Sample GASP-12 was obtained from a quartz-plagioclase-biotite-garnet-sillimanite paragneiss from the LSIMC, located at 42°41′45.47″ S-69°32′37.3″ W (Fig. 2). Automated mineralogical methods (e.g. Fandrich et al., 2007), based on the scanning electron microscope SEM Quanta 650-FEG-MLA (FEI Company) and equipped with Bruker Dual X-Flash energy dispersive spectrometers for EDX analyses, were used to integrate with thin-section information of sample GASP-12 (see Supplementary Material for further detail on methodology). The mineral chemical analyses from sample GASP-12 were performed using a JEOL JXA-8900-RL electron microprobe with beam conditions of 15 kV, 20 nA, and 2 μm, and ZAF correction procedures supplied by JEOL. EPMA (Electron Probe Microanalysis) Th–U–Pb dating is based on the observation that common Pb in monazite (LREE, Th) PO_4 is negligible when compared to radiogenic Pb resulting from the decay of Th and U (Montel et al., 1996). EPMA analysis of the bulk Th, U, and Pb concentrations in monazite, at a constant $^{238}U/^{235}U$, allows for the calculation of a chemical model age (CHIME) with a considerable error (Montel et al., 1996; Pyle et al., 2001; Suzuki and Kato, 2008; Spear et al., 2009). Monazite analyses were performed with an electron microprobe JEOL 8530F at the Helmholtz Institute Freiberg for Resource Technology.

Sample G1 was obtained from a tonalite of PSPC, located at 42°43′48″ S 69°34′ W (Fig. 2). After obtaining grain fractions below 400 μm, the milled sample was processed using conventional isodynamic techniques and zircons were separated from heavy mineral concentrates. Afterwards, zircons were mounted in epoxy resin discs and polished. Before analysis, cathodoluminescence and transmitted images were obtained in order to select the best sites for performing the measurements. These analyses were performed using a Neptune Multi-collector Inductively Coupled Plasma Mass Spectrometer (ICP-MS) and an Analyte G2 excimer Laser Ablation (LA) system at the Centro de Pesquisas Geocronologicas of the Universidade de São Paulo (Brazil). Table S1 provides the cup and ICP-MS configuration and the laser parameters used during the analysis. Supplementary material provides detailed information on methodology. Analytical results are presented in Table S3 of supporting information.

4.2. Electron microprobe analysis and monazite dating

Monazites commonly show complex and patchy zonation patterns and microfracturing revealed by backscattered electron microscopy (Fig. 9a), which are attributed to coupled dissolution-reprecipitation processes. Individual ages span mostly between the Devonian and Early Permian but cannot be correlated with specific zonation patterns. These ages can be grouped into two main populations of 379 ± 5 and 323 ± 5 Ma (Fig. 9b), yet an alternative single age of 348 ± 5 Ma can also be calculated (Fig. S1). The presence of two main age groups seems, however, more likely, and is further supported by minor compositional differences and regional evidence (see Section 5.4). When compared with Carboniferous to Permian ages, Devonian monazite ages commonly show higher UO_2 contents (ca. 0.45–0.72 vs 0.50–0.30 wt %) and generally higher (Th + U)/Si ratios.

4.3. U–Pb LA-ICP-MS zircon geochronology

Sample G1 from the PSPC consists of a mylonitic tonalite, located near the SAP-210 sample, which yields a 314 ± 2 Ma age (Pankhurst et al., 2006). Zircons of sample G1 are typically euhedral and prismatic, with occasionally rounded rims, and exhibit oscillatory zoning (Fig. 10a). In 32 analyses Th/U values range from 0.05 to 0.39 with an average of 0.22. Based on 29 out of 32 analyses, a Tera-Wasserburg diagram was obtained in which two different concordia ages were interpreted. Three analyses were discarded based on their high common Pb or high error ellipses. The remaining 29 analyses are distributed between 336 and 296 Ma (Fig. 10b). From this distribution, a cluster of ten analyses defines a concordia age of 314.1 ± 2.2 Ma (MSWD = 0.00056, probability of concordance = 0.98, Fig. 10c), which is interpreted as the crystallization age. Isolated older zircons present ages of ~336, ~327, ~323, ~319 and are considered as inherited zircon fractions. A younger group of eleven analyses defines a concordia age of 302.8 ± 2.2 Ma (MSWD = 0.13, probability of concordance = 0.72, Fig. 10d), which probably reflects late deformation and re-opening of the isotopic system shortly after emplacement. Samples of similar ages reported by Pankhurst et al. (2006) show a systematic Pb loss, which may reflect deformation conditions present at ~305-300 Ma. In this way, the younger calculated concordia age for G1 sample is considered as a result of mylonitization processes occurred after crystallization, due to chemical variations in zircon crystals that affect U–Pb isotopic systems (Wayne and Sinha, 1988; Hoskin and Schaltegger, 2003). Quartz aggregates showing chessboard extinction patterns, grain boundary migration recrystallization and k-feldpar recrystallization in PSPC (Section 3.2.1, Fig. 7) support high-temperature solid state deformation conditions, and these features commonly occur in temperatures ranging from 500 to 700 °C (Passchier and Trouw, 2005) which could facilitate the re-opening of the isotopic system.

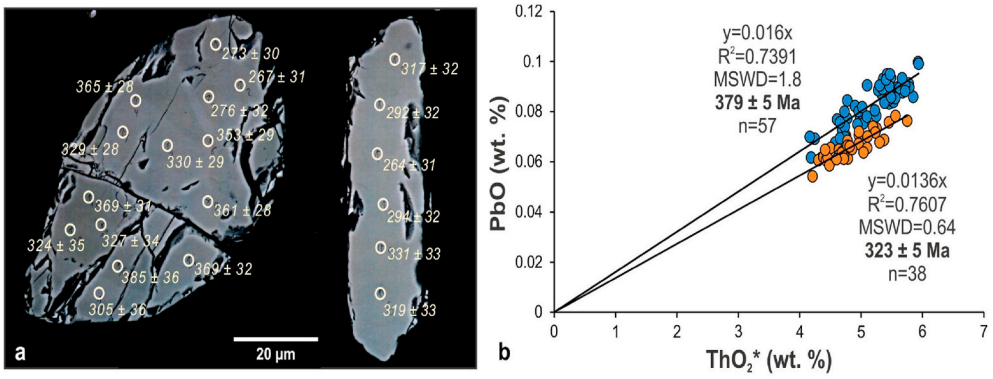

Fig. 9. a) Backscattered electron images (BSE) of monazite showing single Th–U–Pb ages (Ma, 2σ error). b) Th–U–Pb chemical model ages of monazite. Total ThO_2* vs PbO (wt. %) isochrones diagrams. ThO_2* is ThO_2+UO_2 equivalents expressed as ThO_2. Regression lines with the coefficient of determination R^2 are forced through zero (Montel et al., 1996; Suzuki et al., 2008). Weighted average ages (Ma) with MSWD and minimal 2σ error are calculated from single analyses according to Ludwig (2001).

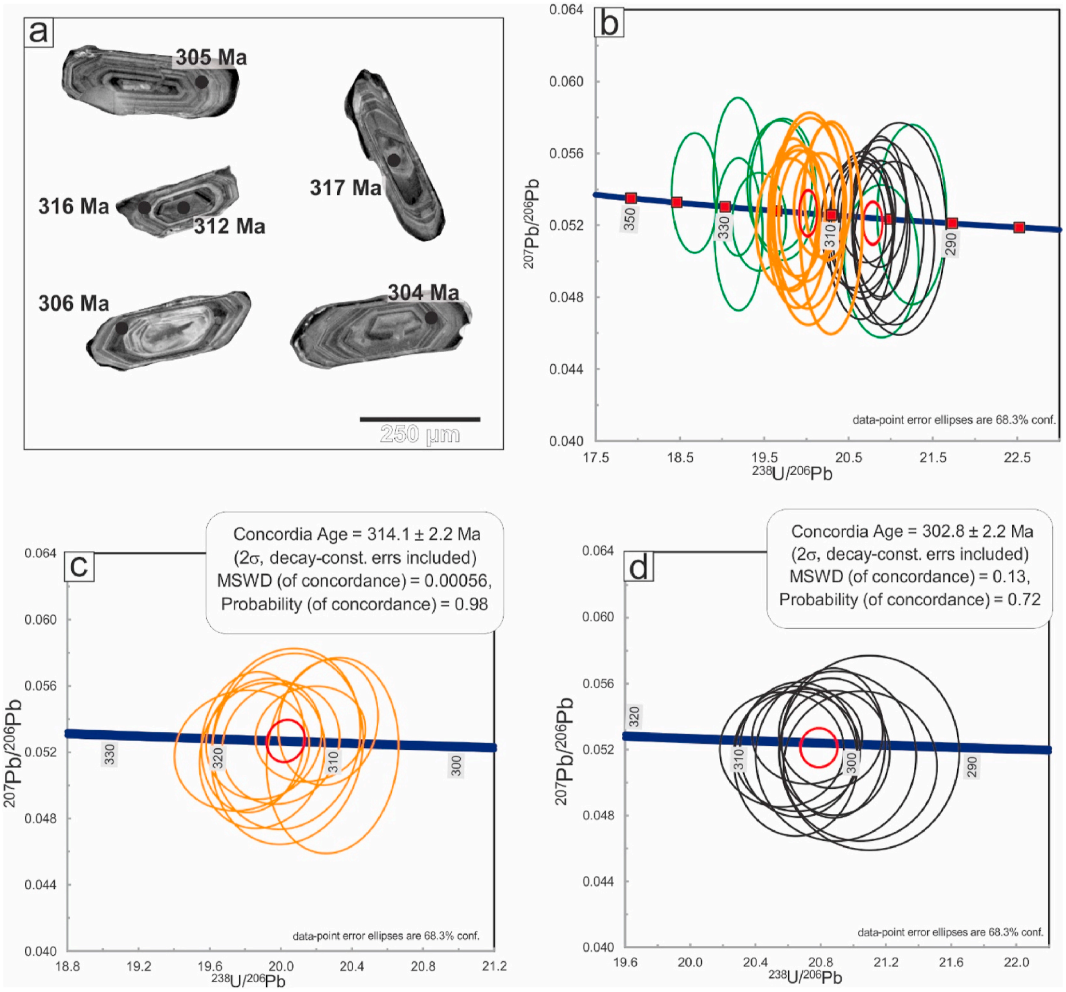

Fig. 10. Cathodoluminescence image and zircon age for sample G1 of the PSPC. a) Cathodoluminescence showing oscillatory zoning in analyzed euhedral prismatic zircons. b) Concordia diagram of zircon U–Pb dating for sample G1. c) Ten analysis defining a concordia age of 314.1 ± 2.2 Ma d) Eleven analysis defining a concordia age of 302.8 ± 2.2 Ma. See text for interpretation.

5. Discussion

5.1. M_1-M_2 metamorphism and associated D_1-D_2 structures

The metamorphic basement of the Taquetrén range comprises a high-grade Igneous-Metamorphic Complex denominated Lagunita Salada Igneous-Metamorphic Complex. A pervasive S_1–S_2 metamorphic foliation with a mean orientation of $S_{1\text{-}2}$: N300°-330°/40°-60°NE is developed in paragneisses, schists and amphibolites, with L_2 mineral stretching lineations exhibiting a moderate plunge to the NE or NNE (Section 3.1.1). Associated with S_1–S_2 foliation, two different sillimanite-bearing mineral assemblages occur among the paragneisses in this Complex. In the northwestern sector, Qtz-Pl-Bt-Grt-Sil paragneisses and in the southern sector of Taquetrén range, garnet paragneisses with a Qtz-Pl-Bt-Grt-Ky-Sil-Kfs-Rt mineral assemblage both exhibiting a well-developed S_1–S_2 fabric. Besides the metapelitic units, amphibolites in the LSIMC show a high-grade mineral assemblage defined by Pl-Amp-Cpx-Opx. Based on the mineral assemblage and paragenesis, these rocks would be the result of a barrovian-type metamorphism in the upper amphibolite to granulite facies developed in pelitic and in mafic protoliths. The absence of primary muscovite and the presence of quartz, sillimanite, and K-feldspar suggest that P-T conditions achieved the second sillimanite reaction-isograd. This is further supported by the presence of orthopyroxene and clinopyroxene along with plagioclase in the amphibolites mineral assemblage which is restricted to the low-pressure part of the granulite facies (Bucher and Grapes, 2011). P-T conditions in a typical metapelitic rock associated with melting have been calculated between 6 and 9 kbar and 750–800° in a Bt-Sil-Kfs-Grt-Pl mineral paragenesis (White et al., 2001).

Electron microprobe Th–U–Pb ages of monazites located in the S_1–S_2 gneissic foliation, display two main populations at 379 ± 5 Ma and 323 ± 5 Ma (Fig. 9b). The obtained spectrum of ages, zonation patterns and the presence of individual monazites with either Devonian or Carboniferous/Early Permian ages suggest long-term high-temperature conditions for the region, mostly between the Late Devonian and Carboniferous. Monazite along S_1–S_2 is considered as stable in middle amphibolite facies for an average pelite composition (Spear, 2009), and is further supported by the presence of individual monazites with either Devonian or Carboniferous/Early Permian ages (Fig. 9a and b).

5.2. Magmatic foliation in the PSPC and D_3 structures in Taquetrén Range

Paso del Sapo Plutonic Complex presents a penetrative NW-SE magmatic/submagmatic foliation which is roughly parallel to the $S_{1\text{-}2}$ structures previously described in the LSIMC. These structures (S_m) are developed in tonalites, granodiorites and K-feldspar porphyric granites. In tonalites and granodiorites, the shape preferred orientation of plagioclases, biotites, and amphiboles define a mean magmatic/submagmatic foliation S_m: N310°/44°NE. In the western part of the plutonic

complex, porphyric K-feldspar granite intrusions are disposed parallel to the penetrative magmatic/submagmatic foliation developed in the granodiorites and tonalites. Shape-preferred orientation of euhedral to subhedral K-feldspar define a S_m: N 321°/40°NE show that S_m magmatic foliation is homogenously developed in the PSPC. Magmatic/submagmatic structures include: a) shape-preferred alignment of hornblende and plagioclase crystals in tonalites and granodiorites and microcline megacrystals in the porphyric granites (Fig. 7a and b), b) submagmatic microfractures, indicating fracturing of plagioclase in the presence of melt (Fig. 7g and h), developed under submagmatic conditions (Bouchez et al., 1992) and c) development of late magmatic shear zones formed in disrupted felsic intrusions (Fig. 6e).

A late deformational stage D_3 affects the LSIMC and the PSPC. This event is developed between D_2 deformational stage and the post-orogenic magmatic intrusion STPC. In the LSIMC these structures are expressed by F_3 asymmetric crenulation folds with a mean fold axis orientation of E_3: N 265°/43° which show a retrograde greenschist facies mineral assemblage defined by Chl + Ser + Ms. In PSPC, D_3 structures are overprinting the described magmatic foliation and are expressed as a pervasive mylonitic foliation developed within discrete shear zones affecting porphyric k-feldspar granites, granodiorites and tonalites of the PSPC. The mylonitic foliation (S_3) presents a mean orientation of S_3: N 321°/40°NE, subparallel to the magmatic/submagmatic foliation S_m. Analyzed microstructures show myrmekites located in the margins of microcline crystal and parallel to S_3 (Fig. 7d), chess-board extinction and grain boundary recrystallization patterns in quartz (Fig. 7c), development of S–C shear bands (Fig. 7f) and pervasive mylonitic fabric (Fig. 7c–h). We consider that the overprinting of initial magmatic foliations occurred by subsequent tectonic processes arisen at high-medium temperature during regional deformation (Paterson et al., 1989) and shortening. This high-temperature solid-state deformation is localized along discrete mylonitic zones developed in PSPC and in some sectors of LSIMC, while low-grade regional metamorphism pervasely affected LSIMC. The D_3 deformational event is probably constrained by the ~303 Ma obtained in the U–Pb analysis (Fig. 10d and Section 5.3). This younger age is interpreted as reflecting pervasive deformation conditions and a re-opening of the isotopic system, in high-temperature conditions, therefore justifying the younger U–Pb ages found in the PSPC (Fig. 10d, Section 4.3; Wayne and Sinha, 1988; Hoskin and Schaltegger, 2003).

5.3. *Summary of deformation, magmatism and metamorphic events in the Taquetrén Range*

Fig. 11 shows a summary of the igneous, metamorphic and deformational events recognized in the Taquetrén range basement. The deposition of the protolith of LSIMC is considered as pre-379 Ma, based on the calculated metamorphic age of 379 ± 5 Ma in monazites of LSIMC paragneiss (Fig. 9). Mineral assemblage in the paragneisses (Qtz-Pl-Bt-Grt-Sil and Qtz-Pl-Bt-Grt-Ky-Sil-Kfs-Rt) and amphibolites (Pl-Amp-Cpx-Opx) indicate high-grade Barrovian-type metamorphism, compatible with amphibolite/lower granulite facies occurred during M_1-M_2 metamorphism. Two different populations of monazites were defined in the PbO–ThO_2 isochrone diagram, defining a 379 ± 5 Ma and a 323 ± 5 Ma ages and suggest high temperature conditions for Late Devonian-Carboniferous times, during M_1-M_2 metamorphic event. Relict D_1 structures are preserved in F_1 isoclinal folds, affected by a NW-SE penetrative S_2 foliation and tight to isoclinal F_2 folds.

Unit	Event	Structure	Metamorphism	Magmatism
Sierra de Taquetrén Plutonic Complex STPC	Post-orogenic intrusion	Non-penetrative magmatic foliation parallel to the pluton margins	-	Magmatic crystallization: post-303 Ma, probably Permian
NW-SE shear zones (affecting PSPC and LSIMC)	D_3-M_3	S_3 crenulation cleavage in LSIMC & S_3 mylonitic foliation in PSPC	Regional low-grade (greenschist facies) in LSIMC; and discrete medium-grade shear zones (amphibolite facies) in PSPC and LSIMC ca. 303 Ma	-
Paso del Sapo Plutonic Complex (PSPC)	Intertectonic emplacement (post-D_2/pre-D_3)	NW-SE magmatic & sub-magmatic foliations (S_m), parallel to S_2 foliation planes	-	Magmatic crystallization: 314 Ma
Lagunita Salada Igneous-Metamorphic Complex (LSIMC)	D_2-M_2	Penetrative; NW-SE-trending S_2 foliation & F_2 tight folds; SW-verging	Medium to high-grade, amphibolite/lower granulite facies 379-323 Ma	-
	D_1-M_1	Relictic; S_1 gneissosity & F_1 isoclinal folds		
	Protolith deposition: >379 Ma	S_0 compositional banding parallel to regional foliations	-	-

Fig. 11. Interpretation of the magmatic, metamorphic and deformational events occurred in the Taquetrén range igneous and metamorphic basement.

At Mid-Carboniferous times, the LSIMC was intruded by the PSPC where a 314.1 ± 2.2 Ma U–Pb (LA-ICP-MS) crystallization age was obtained from a mylonitic tonalite and is interpreted as the age of development of magmatic/submagmatic meso- and micro-scale structures consisting mainly of NW-SE magmatic foliations (S_m) and intramagmatic faults (Figs. 6 and 7). After the intertectonic emplacement of PSPC, a D_3 deformational stage affects regionally the LSIMC and locally, in discrete high-temperature mylonitic zones the PSPC at ca. 303 Ma, based on a 302.8 ± 2.2 U–Pb (LA-ICP-MS) age obtained in a mylonitic tonalite of PSPC and interpreted as the re-opening of the isotopic system and consequent Pb loss induced by the mylonitization process (Fig. 10, Section 4.3). On the other hand, the pervasely D_3 structures affecting LSIMC consist primarily of assymetric crenulation folds affecting S_1–S_2, associated with a retrograde greenschist facies mineral assemblage (Fig. 4d) and minor, discrete NW-SE mylonitic zones. In the PSPC the NW-SE shear zones are expressed in mylonitic k-feldspar granites, tonalites and granodiorites with S–C structures and σ-type k-feldspar porphyroclasts indicating a top-to-the-southwest tectonic transport direction (Fig. 6c and d; Fig. 7). These discrete reverse shear zones, unlike the regional low-grade retrograde metamorphism developed during D_3 in LSIMC, are affected by high temperature deformational processes, which were described in Section 3.2.1 and these conditions probably reopened the isotopic system (Fig. 10). Both the low-grade retrograde metamorphism observed in LSIMC and the discrete high-temperature shear zones recognized in PSPC are not developed in the STPC. In this way and after D_3 deformational event, non-foliated granodiorites and granites of STPC are emplaced with sharp and discordant contacts in the LSIMC host rock. Stoped blocks of PSPC and the lack of deformation in the STPC also suggest a post-D_3 magmatic crystallization (Fig. 11). Considering other non-foliated leucocratic granitoids in the area

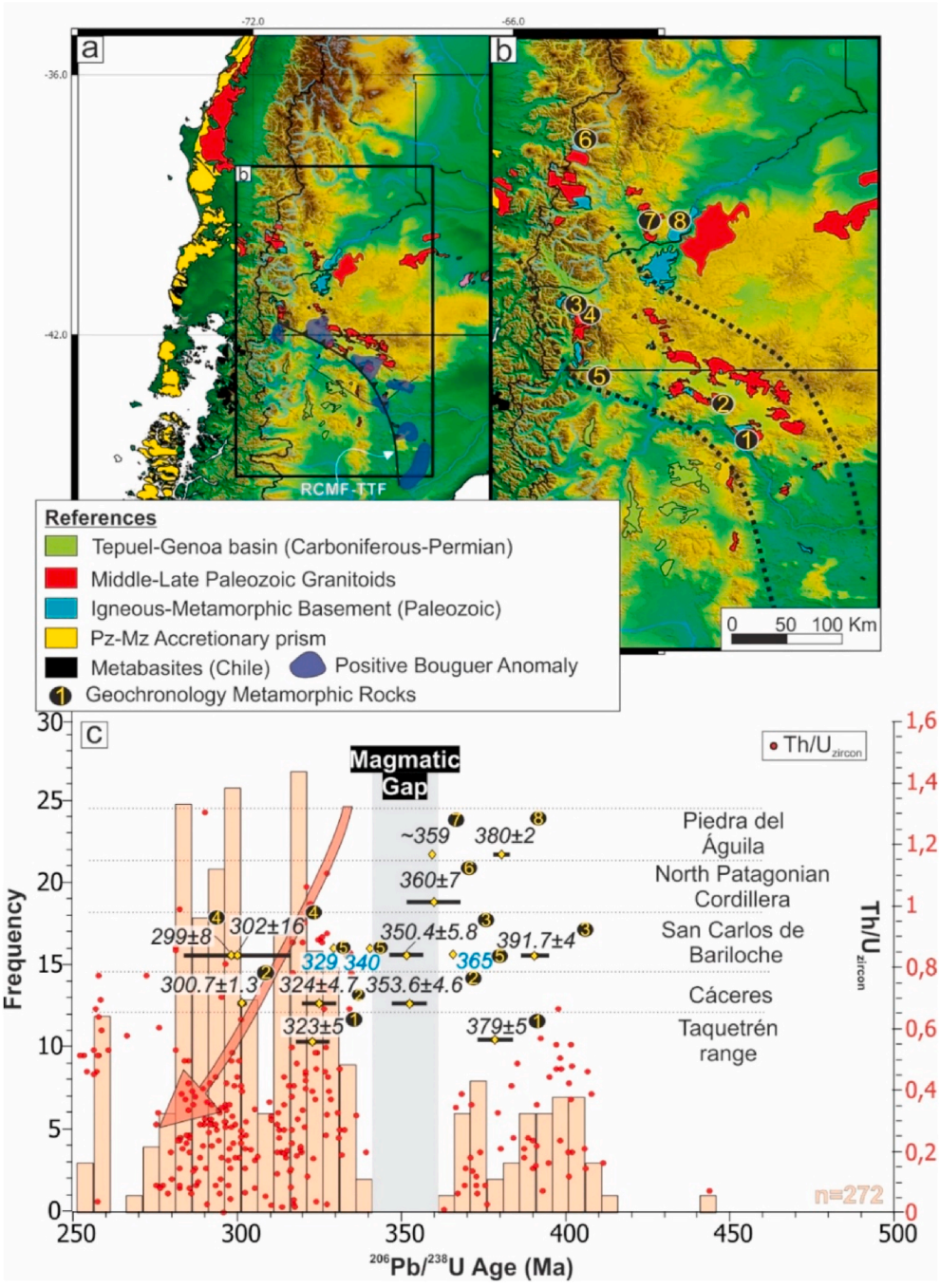

Fig. 12. a) Distribution of Paleozoic lithologies in the region based on Varela et al. (2005), Pankhurst et al. (2006), Ramos (2008) and Hervé et al. (2016). Positive Bouguer anomalies based on Renda et al. (2019). b) Location of the Central Patagonian Igneous-Metamorphic Belt c) Histogram with $^{206}Pb/^{238}U$ ages and Th/U ratios of individual magmatic zircons measured in the southwestern boundary of North Patagonian Massif (based on Pankhurst et al., 2006; Hervé et al., 2018 and this contribution). Metamorphic ages published by different authors: 1. This work, 2. González et al., this contribution, 3. Martínez et al. (2012), 4. Oriolo et al. (2019), 5. Pankhurst et al. (2006), 6. Urraza et al. (2008), 7. Varela et al. (2005), 8. Lucassen et al. (2004).

(Laguna del Toro granodiorite, La Potranca granite, see Pankhurst et al., 2006) a probably Permian age is suggested for this plutonic complex.

5.4. Regional implications

In a regional framework, different igneous-msetamorphic complexes and basement outcrops along the so called "Central Patagonian Igneous-Metamorphic Belt" share strong similarities in their metamorphic mineral assemblages, protoliths, structures, ages of magmatism, and metamorphism. This belt is indicated with dashed line in Fig. 12b. The igneous-metamorphic complexes are located along different high-density basement blocks controlled by different regional-scale structures (e.g. RCMF-TTF in Fig. 12a, see Renda et al., 2019). Metamorphic ages obtained along this belt range from Middle-Late Devonian to Late Carboniferous (Fig. 12b and c). Based on a compilation of previously published data from numerous authors, Fig. 12c shows metamorphic ages and $^{206}Pb/^{238}U$ zircon ages plotted along with Th/U ratios for individual zircons, in order to establish regional correlations and to identify possible tectonic regimes. In our work, a 379 ± 5 Ma Th–U–Pb monazite age was obtained in a paragneiss of Taquetrén Range. For the western area of the North Patagonian Massif, two different Devonian and Carboniferous-Permian igneous-metamorphic events were proposed by Varela et al. (2005) and the ca. 379 Ma age is interpreted as part of the older igneous-metamorphic cycle, which is present in Andean and extra-Andean northern Patagonia. Similar Middle-Late Devonian metamorphic peak ages were obtained in Piedra del Águila and in Bariloche localities (Lucassen et al., 2004; Martinez et al., 2012; Herve et al., 2018, Fig. 12b and c). Coeval magmatism in the North Patagonian Cordillera is represented by the San Martin tonalite, the Lago Lolog granite (401 ± 3 Ma and 395 ± 4 Ma respectively, Pankhurst et al., 2006), the Lago Lolog and Lago Curruhue Chico granodiorites (Hervé et al., 2016) and coeval anatectic granites of ca. 423 Ma (Serra-Varela et al., 2019). In extra-Andean Patagonia, this magmatism is represented by the Colán Conhué and Cáceres granites (394 ± 4 Ma and 371 ± 2 Ma respectively, Pankhurst et al., 2006). Individual $^{206}Pb/^{238}U$ zircon ages show a time span for this magmatism ranging from ~420 to 360 Ma (Fig. 12c).

The Early-Late Devonian magmatism in southwestern North Patagonian Massif ceased at ~360 Ma as is noted by the lack of $^{206}Pb/^{238}U$ zircon ages between 360 and 340 Ma (Fig. 12c). In this way, a ~20 Ma magmatic gap is identified, notably agreeing with a widespread Late Devonian-Early Carboniferous metamorphic event, evidenced in Cáceres (González et al., this contribution), San Carlos de Bariloche (Martinez et al., 2012), North Patagonian Cordillera (Urraza et al., 2008) and probably Piedra del Águila (Varela et al., 2005), as is noted in Fig. 12c. It is important to note that in the latter area, a 348 ± 11 Ma foliated granite was dated by Varela et al. (2005). The presence of a magmatic gap confirms previous proposals of a separation between a Devonian and a Carboniferous-Permian igneous-metamorphic event, denominated "Chanic" and "Gondwanic" respectively by Varela et al. (2005; 2015), which could probably be related to different tectonic settings (Pankhurst et al., 2006; Varela et al., 2015, Marcos et al., 2018).

The 323 ± 5 Ma metamorphic age in Taquetrén range could be correlated with the ca. 324 Ma obtained by González et al. (this contribution) in the high-grade Cáceres Igneous-Metamorphic Complex, suggesting a ca. 330–320 regional metamorphism, coeval with syntectonic magmatism (~330-300 Ma). The Carboniferous-Permian magmatism spanning from ~340 to 270 Ma is represented by I- and S-type syntectonic granitoids spanning from ~330 to 300 Ma while post-tectonic peraluminous magmatism spans from ~290 to 270 Ma (Pankhurst et al., 2006). Based on the structural analysis presented in this work, the syntectonic structural characteristic of the 314.1 ± 2.2 Ma tonalite in the Paso del Sapo Complex was confirmed and interpreted in a context of crustal thickening and ~NE-SW tectonic contraction with a top-to-the-southwest tectonic transport direction. Late Carboniferous deformation is suggested by the 302.8 ± 2 Ma calculated concordia age for the PSPC, indicating the ongoing Late Carboniferous thickening process along the belt as it was previously proposed in Río Chico (Hervé et al., 2005), Bariloche (Oriolo et al., 2019) and near Comallo (Marcos et al., 2020) localities. In this sense, regional Th/U ratios of individual zircons show a decreasing trend from the Early Carboniferous to the Early Permian, from 1.2 to 1.4 to <0.8 (Fig. 12c). Shifts in zircon Th/U values may reflect different tectonic conditions in magmatism, where lower zircon Th/U values could indicate a contractional tectonic setting (McKay et al., 2018 and references therein). This crustal thickening process controlling part of the ~340-270 Ma magmatism is further evidenced by Sr/Y ratios in granitoids associated with NW-SE Late Carboniferous deformational fabrics in metamorphic rocks (Oriolo et al., 2019) and was also suggested by different authors in the western part of North Patagonian Massif (Dalla Salda et al., 1994; Cerredo and Lopez de Luchi, 1998; Giacosa et al., 2004).

Previous geotectonic models propose a continuous Paleozoic magmatic arc spanning from ~400 to 320 Ma in Central Patagonia, denominated the "Western Magmatic Arc" (Ramos, 2008). However, the compilation of magmatic and metamorphic ages (Fig. 12c) reveals, at least, two different Paleozoic magmatic episodes present in Central Patagonia, related with medium- to high-grade barrovian metamorphism: the Chanic magmatism spanning from ~400 to 360 Ma and the Gondwanic magmatism spanning from ~330 to 270 Ma. A similar appreciation was made by Varela et al. (2015) based on the geochemical differentiation of both episodes. In the Gondwanic magmatic cycle, syntectonic magmatism spans from ~330 to 300 Ma, whereas post-tectonic Permian granitoids are still controlled by previous inherited metamorphic fabrics but are emplaced in a waning orogenic to post-orogenic tectonic context. In Taquetren Range, this is represented by the Sierra de Taquetrén Plutonic Complex, consisting of peraluminous, structurally discordant intrusions.

A similar characterization of Gondwanic magmatism was made by Pankhurst et al. (2006) based on geochemical data, though they propose the collision of the Deseado Massif at 320-310 Ma, relating the 335-320 Ma I-type magmatism with a pre-collisional subduction stage. On the other hand, the Antarctic Peninsula (Ramos, 2008) was also suggested as a potential collisional block as it shares a common Permian-Triassic tectono-magmatic evolution with Patagonia (Heredia et al., 2018; Suarez et al., 2019). In recent years, a 385-360 Ma oceanic terrane named "Chaitenia" was defined in the Chilean accretionary prism (Hervé et al., 2016, 2018), immediately to the southwest of the so-called "Central Patagonian Igneous-Metamorphic Belt" (metabasites in Fig. 12a) and we consider it as a potential accreted terrain responsible of widespread deformation in Middle-Late Paleozoic times in the Central Patagonian Igneous-Metamorphic Belt, coeval with the metamorphism and the associated magmatic gap described. Alternatively, the southwestern boundary of the North Patagonian Massif was considered as a transcontinental deformation belt for Late Paleozoic times, related to an intragondwanan weak lithospheric zone (Vizán et al., 2017). Besides the geotectonic model proposed to explain the deformational belt located in this area, future models should consider the magmatic gap of ~20 My derived from U–Pb zircon ages (Fig. 12c) for Late Devonian - Early Carboniferous times (360-340 Ma) and its correlation with medium-to high-grade metamorphism (~350 Ma, Fig. 12c). For such a model, a crustal thickening process can be related to the interruption of continental magmatism, and a common geotectonic framework probably triggers both phenomena. Following this magmatic gap, increased crustal thickening due to stacking of crustal nappes and posterior thermal relaxation would probably generate the anatexis of lower crustal components tens of millions of years after the crustal thickening event, which is a common occurrence in magmatism after thickened orogens (England and Thompson, 1984; Nédélec and Bouchez, 2015). Part of the I- and S-type Late Carboniferous syntectonic magmatism and subsequent post-tectonic peraluminous granites (Pankhurst et al., 2006) could be related to this process.

6. Conclusions

Combined structural, microstructural and geochronological analyses in the igneous-metamorphic basement of Taquetrén Range (Central Patagonia, Argentina), allowed the definition of three new basement units called the Lagunita Salada Igneous-Metamorphic Complex, Paso del Sapo Plutonic Complex, and Sierra de Taquetrén Plutonic Complex. The Lagunita Salada Igneous-Metamorphic Complex (LSIMC) is formed by paragneisses, schists, migmatites, and minor bodies of amphibolites. S_1–S_2 represents the main metamorphic foliation: N315°-350°/30°-72°NE, associated with Qtz-Pl-Bt-Grt-Sil and Qtz-Pl-Bt-Grt-Ky-Sil-Kfs-Rt mineral assemblages in paragneisses. Based on previously calculated P-T conditions for average pelite compositions, possible metamorphic conditions of 6–9 kbar and 650–800 °C, related with upper-amphibolite to granulite facies metamorphism are suggested. The timing of peak upper amphibolite to granulite conditions are constrained by an EPMA Th–U–Pb monazite ages of 379 ± 5 Ma and 323 ± 5 Ma, which suggest long-term high-temperature conditions for the region, mostly between the Late Devonian and Carboniferous. These conditions are coherent with the production of coeval or slightly younger anatexis of paragneisses forming the associated metatexites.

On the other hand, the Paso del Sapo Plutonic Complex (PSPC) intrudes the LSIMC and shows structural and microstructural evidence that suggests an emplacement under regional contractional conditions. Foliations and lineations show continuity within the wall rocks and the granitoids of this Complex. An LA-ICP-MS U–Pb zircon age of 314.1 ± 2.2 Ma was obtained in foliated tonalite of the PSPC, confirming a previous ~314 Ma U–Pb zircon age obtained by Pankhurst et al. (2006) in a close location. A second concordia age of 302.8 ± 2.2 Ma was interpreted as partial re-equilibration of zircons under high-temperature deformation conditions, hence suggesting the persistence of relatively high-strain until Late Carboniferous times. Differences in structural data along Taquetrén range could be related with strain partitioning between metamorphic rocks and related syntectonic intrusions. Besides minor structural differences between LSIMC and PSPC, both units show a well-developed NW-SE foliation with moderate to steep inclinations towards the NE and the observed direction of tectonic transport is top-to-the-SW.

Based on previously published U–Pb zircon ages, syntectonic Late Paleozoic magmatism in Central Patagonia starts after a ~20 My magmatic gap period (360-340 Ma), in which amphibolite-granulite facies metamorphism is developed in different sectors of the so-called Central Patagonian Igneous-Metamorphic Belt. While dissimilar tectonic settings have been proposed for the Paleozoic igneous-metamorphic belt in Central Patagonia, future models should consider the ~350 Ma peak metamorphic conditions in upper amphibolite-granulite facies, located in different sectors of the belt and its association with the ~20 Ma magmatic gap distributed along the southwestern margin of North Patagonian Massif.

Declaration of competing interest

The authors declare that they have no known competing financial interests or personal relationships that could have appeared to influence the work reported in this paper.

Acknowledgements

Special thanks for financial support of Agencia Nacional de Promoción Científica y Tecnológica (PICT2017-0709 and PICT-2017-1092), Universidad de Buenos Aires (UBACyT 20020150100069BA) and the National Geographic Society (grant CP-123R-17). The automated SEM-MLA and EPMA microprobe analyses at TU Bergakademie Freiberg/Saxony were assisted by Sabine Gilbricht. We thank Dr. E. A. Cristofolini and Dr. L. Pinotti for their thoughtful comments which helped in improving this work. This work could not have been done without the support of local inhabitants of Paso del Sapo locality and specially of Juan E. Giacomino Cunningham. Dedicated to Dr. Rubén Somoza.

Appendix J. Supplementary data

Supplementary data to this article can be found online at https://doi.org/10.1016/j.jsames.2020.103045.

References

Bilmes, A., DÉlia, L., Franzese, J.R., Veiga, G.D., Hernández, M., 2013. Miocene block uplift and basin formation in the Patagonian foreland: the Gastre Basin, Argentina. Tectonophysics 601 (98), 111. https://doi.org/10.1016/j.tecto.2013.05.001.

Bohlen, S.R., Mezger, K., 1989. Origin of granulite terranes and the formation of the lowermost continental crust. Science 244, 326–329.

Bouchez, J.L., Delas, C., Gleizes, G., Nédélec, A., 1992. Submagmatic microfractures in granites. Geology 20 (1), 35–38. https://doi.org/10.1130/00917613(1992)020<0035:SMIG>2.3.CO;2.

Bucher, K., Grapes, R., 2011. Petrogenesis of Metamorphic Rocks. Springer-Verlag, Berlin-Heiderberg.

Bucher, J., García, M., López, M., Milanese, F., Bilmes, A., D'Elia, L., Naipauer, M., Sato, A.M., Funes, D., Rapalini, A., Franzese, J., 2019. Tectonostratigraphic evolution and timing deformation in the Miocene Paso del Sapo Basin: implications for the Patagonian Broken Foreland. J. South Am. Earth Sci. 94, 102212.

Busteros, A., Lema, R. Giacosa y H., 1998. Hoja 4166-IV – Sierra Grande, Provincia de Río Negro. Servicio Geológico Minero Argentino. Boletín 241, Buenos Aires.

Caminos, R., 1983. Descripción geológica de las Hojas 39 g, Cerro Tapiluke y 39 h, Chipauquil, provincia de Río Negro. Servicio Geológico Nacional, (inédito), 41p., Buenos Aires.

Coira, B.L., Nullo, F.E., Proserpio, C., Ramos, V.A., 1975. Tectónica de basamento de la región Occidental del Macizo Nordpatagónico, provincias de Río Negro y Chubut. Rev. Asoc. Geol. Argent. 30 (4), 361–383.

Cerredo, M.E., López De Luchi, M.G., 1998. Mamil choique granitoids, southwestern North Patagonian Massif, Argentina: magmatism and metamorphism associated with a polyphasic evolution. J. South Am. Earth Sci. 11, 499–515. https://doi.org/10.1016/S0895-9811(98)00025-X.

Ciccioli, P.L., Limarino, C.O., Isbell, J.L., Taboada, A.C., Pagani, M.A., Gulbranson, E.L., 2020. Interpreting detrital modes and geochemistry of sandstones from the late Paleozoic Tepuel-Genoa Basin: paleogeographic implications (Patagonia, Argentina). J. S. Am. Earth Sci. 102858.

Cisneros-Lazaro, D.G., Miller, J.A., Baumgartner, L.P., 2019. Role of myrmekite and associated deformation fabrics in controlling development of granitic mylonites in the Pofadder Shear Zone of southern Namibia. Contrib. Mineral. Petrol. 174, 22. https://doi.org/10.1007/s00410-019-1555-9.

Dalla Salda, L.H., Varela, R., Cingolani, C., Aragón, E., 1994. The rio Chico paleozoic crystalline complex and the evolution of northern Patagonia. J. South Am. Earth Sci. 7, 377–386. https://doi.org/10.1016/0895-9811(94)90022-1.

Echaurren, A., Folguera, A., Gianni, G., Orts, D., Tassara, A., Encinas, A., Giménez, M., Valencia, V., 2016. Tectonic evolution of the North Patagonian Andes (41–44 S) through recognition of syntectonic strata. Tectonophysics 677–678, 99–114.

England, P.C., Thompson, A.B., 1984. Pressure-temperature-time paths of regional metamorphism I. Heat transfer during the evolution of regions of thickened continental crust. J. Petrol. 25 (4), 894–928.

Fandrich, R., Gu, Y., Burrows, D., Moeller, K., 2007. Moder SEM-based mineral liberation analysis. Int. J. Miner. Process. 84, 310–320.

Figari, E.G., 2005. Evolución Tectónica de la Cuenca Cañadón Asfalto. (Zona del valle medio del río Chubut). Facultad de Ciencias Exactas y Naturales, Universidad de Buenos Aires, p. 106.

Feruglio, E., 1949. Rocas cristalinas de la Patagonia extra-Andina. In: Ferugio, E. (Ed.), Descripción geológica de la Patagonia. Dirección General de YPF, Ministerio de Industria y Comercio de la Nación. Tomo I (Capítulo III), pp. 26–32 (Buenos Aires).

Figari, E.G., Scasso, R.A., Cúneo, R.N., Escapa, I., 2015. Estratigrafía y evolución geológica de la cuenca de cañadón asfalto, provincia de Chubut, Argentina. Lat. Am. J. Sedimentol. Basin Anal. 22, 11–70.

Foix, N., Allard, J.O., Ferreira, M.L., Atencio, M., 2020. Spatio-temporal variations in the mesozoic sedimentary record, golfo san jorge basin (Patagonia, Argentina): andean vs cratonic sources. J. S. Am. Earth Sci. 102464.

Folguera, A., Ramos, V.A., 2011. Repeated eastward shifts of arc magmatism in the Southern Andes: a revision to the long-term pattern of Andean uplift and magmatism. J. South Am. Earth Sci. 32, 531–546. https://doi.org/10.1016/j.jsames.2011.04.003.

Fountain, D.M., Salisbury, M.H., 1981. Exposed cross-sections through the continental crust: implications for crustal structure, petrology, and evolution. Earth Planet Sci. Lett. 56, 263–277.

Giacosa, R., 1987. Caracterización de un sector del basamento metamórfico- migmatítico en el extremo suroriental del Macizo Norpatagónico, provincia de Río Negro, Argentina. Actas 10° Congreso Geológico Argentino 3, 51–54 (Buenos Aires).

Giacosa, R., Márquez, M., Nillni, A., Fernández, M., Fracchia, D., Parisi, C., Afonso, J., Paredes, J., Sciutto, J., 2004. Litología y estructura del basamento ígneo-metamórfico del borde SO del Macizo Nordpatagónico al oeste del río Chico, (Cushamen, Chubut, 42° 10′S - 70° 30′O). Rev. la Asoc. Geol. Argentina 59, 569–577.

Giacosa, R.E., González, P.D., Silva Nieto, D., Busteros, A., Lagorio, S., Rossi, A., 2014. Complejo Ígneo-Metamórfico Cáceres: Una nueva unidad metamórfica de alto grado en el basamento de Gastre, Macizo Nordpatagónico (Chubut). XIX Congreso Geológico Argentino, Tectónica Preandina.

Giacosa, R.E., 2020. Basement control, sedimentary basin inception and early evolution of the Mesozoic basins in the Patagonian foreland. J. S. Am. Earth Sci. 102407.

González, P.D., Sato, A.M., Naipauer, M., Varela, R., Basei, M., Sato, K., Llambías, E.J., Chemale, F., Dorado, A.C., 2018. Patagonia-Antarctica Early Paleozoic conjugate margins: cambrian synsedimentary silicic magmatism, U-Pb dating of Kbentonites, and related volcanogenic rocks. Gondwana Res. 63, 186–225. https://doi.org/10.1016/J.GR.2018.05.015.

González P., Giacosa R., Lagorio S., Busteros A., Sato A. M., Justiniano C. B., Basei M. A. S., Silva Nieto D. This issue. U-Pb geochronology of the igneous-metamorphic basement of central Patagonia: constraints on the timing of Paleozoic tectono-metamorphic evolution.

Greco, G.A., González, P.D., González, S.N., Sato, A.M., Basei, M.A.S., Tassinari, C.C.G., Sato, K., Varela, R., Llambías, E.J., 2015. Geology, structure, and age of the nahuel niyeu formation in the aguada cecilio area, North Patagonian massif, Argentina. J. S. Am. Earth Sci. 62, 12–32.

Heredia, N., García-Sansegundo, J., Gallastegui, G., Farias, P., Giacosa, R.E., Hongn, F.D., Tubía, J.M., Alonso, J.L., Busquets, P., Charrier, R., Clariana, P., Colombo, F., Cuesta, A., Gallastegui, J., Giambiagi, L.B., González-Menéndez, L., Limarino, C.O., MartínGonzález, F., Pedreira, D., Quintana, L., Rodríguez-Fernández, L.R., Rubio-Ordóñez, A., Seggiaro, R.E., Serra-Varela, S., Spalletti, L.A., Cardó, R., Ramos, V.A., 2018. The Pre-Andean phases of construction of the Southern Andes basement in Neoproterozoic-Paleozoic times. In: The Evolution of the Chilean-Argentinean Andes. Springer, Cham, pp. 111–131.

Hervé, F., Calderon, M., Fanning, C.M., Pankhurst, R.J., Fuentes, F., Rapela, C.W., 2016. Devonian magmatism in the accretionary complex of southern Chile. J. Geol. Soc. 173 (4), 587–602. https://doi.org/10.1144/jgs2015-163.

Hervé, F., Calderon, M., Fanning, C.M., Pankhurst, R.J., Rapela, C.W., Quezada, P., 2018. The country rocks of Devonian magmatism in the north Patagonian massif and Chaitenia. Andean Geol. 45 (3), 301–317. https://doi.org/10.5027/andgeoV45n3-3117.

Hervé, F., Haller, M.J., Duhart, P., Fanning, C.M., 2005. SHRIMP U-Pb ages of detrital zircons from cushamen and esquel formations, North Patagonian massif, Argentina: geological implications. In: Congreso Geológico Argentino, No. 16. Actas, La Plata, pp. 309–314.

Hoskin, P.W.O., Shaltegger, U., 2003. The composition of zircon and igneous and metamorphic petrogenesis. In: Hanchar, J.M., Hoskin, P.W.O. (Eds.), Zircon. Reviews in Mineralogy and Geochemistry, vol. 53. Mineralogical Society of America, Washington, DC, pp. 27–62.

Lesta, P., Ferello, R., Chebli, G., 1980. Chubut extraandino. In: Segundo Simposio Geología Regional Argentina, vol. 2. Academia Nacional de Ciencias, Córdoba, pp. 1306–1387.

Limarino, C.O., Spalletti, 2006. Paleogeography of the upper Paleozoic basins of southern South America: an overview. J. S. Am. Earth Sci. 22, 134–155.

Linares, E., González, R.R., 1990. Catálogo de edades radimétricas de la República Argentina 1957-1987. In: Asociación Geológica Argentina, vol. 19. Publicaciones Especiales Serie B, Didáctica y Complementaria, p. 628.

Lucassen, F., Trumbull, R., Franz, G., Creixell, C., Vásquez, P., Romer, R.L., Figueroa, O., 2004. Distinguishing crustal recycling and juvenile additions at active continental margins: the Paleozoic to recent compositional evolution of the Chilean Pacific margin (36–41 S). J. S. Am. Earth Sci. 17 (2), 103–119.

Marcos, P., Gregori, D.A., Benedini, L., Barros, M., Strazzere, L., Pavón Pivetta, C., 2018. Pennsylvanian glacimarine sedimentation in the Cushamen Formation, western north Patagonian massif. Geoscience Frontiers 9 (2), 485–504. https://doi.org/10.1016/j.gsf.2017.05.005.

Marcos, P., Pivetta, C.P., Benedini, L., Gregori, D.A., Mauro, C.G., Scivetti, N., Barros, M., Varela, M.E., Dos Santos, A., 2020. Late Paleozoic geodynamic evolution of the western North Patagonian Massif and its tectonic context along the southwestern Gondwana margin. LITHOS. https://doi.org/10.1016/j.lithos.2020.105801.

Martínez, J.C., Dristas, J.A., Massonne, H.-J., 2012. Palaeozoic accretion of the microcontinent Chilenia, North Patagonian Andes:high-pressure metamorphism and subsequent thermal relaxation. Int. Geol. Rev. 54 (4), 472–490. https://doi.org/10.1080/00206814.2011.569411.

McKay, M.P., Jackson Jr., W.T., Hessler, A.M., 2018. Tectonic stress regime recorded by zircon Th/U. Gondwana Res. 57, 1–9.

Montel, J.M., Foret, S., Veschambre, M., Nicollet, C., Provost, A., 1996. Electron microprobe dating of monazite. Chem. Geol. 131 (1-4), 37–53. https://doi.org/10.1016/0009-2541(96)00024-1.

Nakayama, C., 1973. Sedimentitas pre-bayocianas en el extremo austral de la sierra de Taquetrén, Chubut (Argentina). Act. Quinto Congr. Geol. Arg. III, 269–277.

Nédélec, A., Bouchez, J.L., 2015. Granites: Petrology, Structure, Geological Setting, and Metallogeny. Oxford University Press, Oxford, p. 335.

Oriolo, S., Schulz, B., González, P.D., Bechis, F., Olaizola, E., Krause, J., Renda, E.M., Vizán, H., 2019. The late paleozoic tectonometamorphic evolution of Patagonia revisited: insights from the pressure-temperature-deformation-time (P-T-D-t) path of the gondwanide basement of the north patagonian Cordillera (Argentina). Tectonics. https://doi.org/10.1029/2018TC005358.

Pángaro, F., Ramos, V.A., 2012. Paleozoic crustal blocks of onshore and offshore central Argentina: new pieces of the southwestern Gondwana collage and their role in the accretion of Patagonia and the evolution of Mesozoic south Atlantic sedimentary basins. Mar. Petrol. Geol. 37, 162–183.

Pankhurst, R.J., Rapela, C.W., Fanning, C.M., Márquez, M., 2006. Gondwanide continental collision and the origin of Patagonia. Earth Sci. Rev. 76, 235–257. https://doi.org/10.1016/j.earscirev.2006.02.001.

Pankhurst, R.J., Rapela, C.W., López de Luchi, M.G., Rapalini, A.E., Fanning, C.M., Galindo, C., 2014. The Gondwana connections of northern Patagonia. J. Geol. Soc. 171, 313–328. https://doi.org/10.1144/jgs2013-081.

Paterson, S.R., Vernon, R.H., Tobish, O.T., 1989. A review of criteria for the identification of magmatic and tectonic foliations in granitoids. J. Struct. Geol. 11, 349–363.

Prezzi, C., Vizán, H., Vázquez, S., Renda, E.M., Oriolo, S., Japas, M., 2018. Evolution of the Paleozoic Claromecó Basin (Argentina) and geodynamic implications for the southwestern margin of Gondwana: insights from isostatic, gravimetric and magnetometric models. Tectonophysics 742. https://doi.org/10.1016/j.tecto.2018.05.025.

Pyle, J.M., Spear, F.S., Rudnick, R.L., McDonough, W.F., 2001. Monazite-xenotime-garnet equilibrium in metapelites and a new monazite-garnet thermometer. J. Petrol. 42 (11), 2083–2107. https://doi.org/10.1093/petrology/42.11.2083.

Ramos, V.A., 1975. Geología del sector orientaldel Macizo Nordpatagónico entre Aguada Capitán y la Mina Gonzalito, provincia de RíoNegro. Rev. Asoc. Geol. Argent. 30 (3), 274–285.

Ramos, V.A., 1984. Patagonia: ¿un continente paleozoico a la deriva? IX. Congreso Geológico Argentino, vol. 2. San Carlos de Bariloche, Actas, pp. 311–325.

Ramos, V.A., 1999. Las provincias geológicas del territorio argentino. In: Caminos, R. L.702 (Ed.), Geología Argentina, vol. 29. SEGEMAR, Anales, pp. 41–96.

Ramos, V.A., 2008. Patagonia: a Paleozoic continent adrift? J. S. Am. Earth Sci. 26, 235–251.

Ramsay, J.G., 1967. Folding and Fracturing of Rocks. McGraw-Hill, New York, p. 568.

Rapalini, A.E., López de Luchi, M., Tohver, E., Cawood, P.A., 2013. the South American ancestry of the north patagonian massif: geochronological evidence for an autochthonous origin? Terra. Nova 25, 337–342. https://doi.org/10.1111/ter.12043.

Ravazzoli, I.A., Sesana, F.L., 1977. Descripción geológica de la Hoja 41c "río Chico" (1: 200.000), provincia de Río negro. Servicio Geológico Nacional, Boletín N° 148, 1–77.

Renda, E.M., Oriolo, S., Vizán, H., 2017. Comparación estructural entre dos unidades de la Formación Mamil Choique: Granitoide de Sierra del Medio (~253 Ma) y granodiorita Paso del Sapo (~314 Ma), vol. 13. XX Congreso Geológico Argentino, Simposio, pp. 141–145.

Renda, E.M., Álvarez, D., Prezzi, C., Oriolo, S., Vizán, H., 2019. Inherited basement structures and their influence in foreland evolution: a case study in Central Patagonia, Argentina. Tectonophysics 772. https://doi.org/10.1016/j.tecto.2019.228232.

Ruiz González, V., Puigdomenech, C.G., Zaffarana, C.B., Vizán, H., Somoza, R., 2020. Paleomagnetic evidence of the brittle deformation of the central patagonian batholith at gastre area (Chubut province, Argentina). J. S. Am. Earth Sci. 98, 102442.

Serra-Varela, S, González, P.D., Giacosa, R.E., Heredia, N., Pedreira, D., Martín-González, F., Sato, A.M., 2019. Evolution of the Palaeozoic basement of the North Patagonian Andes in the San Martín de los Andes area (Neuquén, Argentina): petrology, age and correlations. Andean Geol. 46 (1), 102–130. https://doi.org/10.5027/andgeoV46n1-3124.

Simpson, C., Wintsch, R.P., 1989. Evidence for deformation-induced K-feldspar replacement by myrmekite. J. Metamorph. Geol. 7, 261–275.

Spear, F., Pyle, J., Cherniak, D., 2009. Limitations of chemical dating monazite. Chem. Geol. 266, 218–230. https://doi.org/10.1016/j.chemgeo.2009.06.007.

Suárez, R., González, P.D., Ghiglione, M.C., 2019. A review on the tectonic evolution of the Paleozoic-Triassic basins from Patagonia: record of protracted westward migration of the pre-Jurassic subduction zone. J. S. Am. Earth Sci. 102256.

Suzuki, K., Kato, T., 2008. CHIME dating of monazite, xenotime, zircon and polycrase: protocol, pitfalls and chemical criterion of possibly discordant age data. Gondwana Res. 14, 569–586. https://doi.org/10.1016/j.gr.2008.01.005.

Turner, J.C.M., 1965. Estratigrafía de la comarca de Junín de los Andes. Academia Nacional de Ciencias Boletín 44, 5–51 (Córdoba).

Uriz, N.J., Cingolani, C.A., Chemale, F.J., Macambira, M.B., Armstrong, R., 2011. Isotopic studies on detrital zircons of Silurian–Devonian siliciclastic sequences from Argentinean North Patagonia and Sierra de la Ventana regions: comparative provenance. Int. J. Earth Sci. 100, 571–589. https://doi.org/10.1007/s00531-010-0597-z.

Urraza, I.A., Grecco, L.E., Delpino, S.H., Arrese, M.L., 2008. Determination of Rock Ages by Chemical Analysis of Th, U, Pb in the Mineral Monazite (Ce, La, Th, REE, U)PO4 Using EPMA. Paper presented at Annual General Meeting and Research Day, Halifax, Canada.

Varela, R., Basei, M.A.S., Cingolani, C.A., Siga Jr., O., Passarelli, C.R., 2005. El Basamento Cristalino de los Andes norpatagónicos en Argentina: geocronología e interpretación tectónica. Rev. Geol. Chile 32, 167–182.

Varela, R., Gregori, D.A., González, P.D., Basei, M.A.S., 2015. Caracterización geoquímica del magmatismo de arco Devónico y Carbonífero-Pérmico en el Noroeste de Patagonia. Rev. Asoc. Geol. Argent. 72, 419–432.

Vizán, H., Prezzi, C.B., Geuna, S.E., Japas, M.S., Renda, E.M., Franzese, J., Van Zele, M. A., 2017. Paleotethys slab pull, self-lubricated weak lithospheric zones, poloidal and toroidal plate motions, and Gondwana tectonics. Geosphere 13 (5), 1541–1554. https://doi.org/10.1130/GES01444.1.

Volkheimer, W., 1964. Estratigrafía de la zona extraandina del Departamento de Cushamen (Chubut) entre los paralelos 42° y 42° 30' y los meridianos 70° y 72°. Rev. Asoc. Geol. Argent. 19 (2), 85–107.

Wayne, D.M., Sinha, A.K., 1988. Physical and chemical response of zircons to deformation. Contrib. Mineral. Petrol. 98, 109–121.
White, R.W., Powell, R., Holland, T.J.B., 2001. Calculation of partial melting equilibria in the system Na_2O-CaO-K_2O-FeO-MgO-Al_2O_3-SiO_2-H_2O (NCKFMASH). J. Metamorph. Geol. 19, 139–153.
Whitney, D.L., Evans, B.W., 2010. Abbreviations for names of rock-forming minerals. Am. Mineral. 95, 185–187.
Yoshino, T., Okudaira, T., 2004. Crustal growth by magmatic accretion constrained by metamorphic P-T paths and thermal models of the kohistan arc, NW himalayas. J. Petrol. 45 (11), 2287–2302.
Zaffarana, C.B., Somoza, R., Orts, D.L., Mercader, R., Boltshauser, B., González, V.R., Puigdomenech, C., 2017. Internal structure of the late triassic central patagonian batholith at gastre, southern Argentina: implications for pluton emplacement and the gastre fault system. Geosphere 13, 1973–1992. https://doi.org/10.1130/GES01493.1.